Statistical Analysis of the Relation between Coronal Mass Ejections and Solar Energetic Particles

Kosuke Kihara,[1] Yuwei Huang,[1] Nobuhiko Nishimura,[2] Nariaki V. Nitta,[3] Seiji Yashiro,[4] Kiyoshi Ichimoto,[1] and Ayumi Asai[1]

[1]*Astronomical Observatory, Kyoto University, Sakyo, Kyoto 606-8502, Japan*
[2]*Institute for Space-Earth Environmental Research, Nagoya University, Nagoya, Japan*
[3]*Lockheed Martin Solar and Astrophysics Laboratory, Palo Alto, CA 94304 USA*
[4]*Department of Physics, The Catholic University of America, Washington, USA*

Submitted to ApJ

ABSTRACT

To improve the forecasting capability of impactful solar energetic particle (SEP) events, the relation between coronal mass ejections (CMEs) and SEP events needs to be better understood. Here we present a statistical study of SEP occurrences and timescales with respect to the CME source locations and speeds, considering all 257 fast ($v_{CME} \geq 900$ km s^{-1}) and wide (angular width $\geq 60°$) CMEs that occurred between December 2006 and October 2017. We associate them with SEP events at energies above 10 MeV. Examination of the source region of each CME reveals that CMEs more often accompany a SEP event if they originate from the longitude of E20 − W100 relative to the observer. However, a SEP event could still be absent if the CME is < 2000 km s^{-1}. For the associated CME-SEP pairs, we compute three timescales for each of the SEP events, following Kahler (2005, 2013); namely the timescale of the onset (TO), the rise time (TR), and the duration (TD). They are correlated with the longitude of the CME source region relative to the footpoint of the Parker spiral ($\Delta\Phi$) and v_{CME}. The TO tends to be short for $|\Delta\Phi| < 60°$. This trend is weaker for TR and TD. The SEP timescales are only weakly correlated with v_{CME}. Positive correlations of both TR and TD with v_{CME} are seen in poorly connected (large $|\Delta\Phi|$) events. Additionally, TO appears to be negatively correlated with v_{CME} for events with small $|\Delta\Phi|$.

Keywords: coronal mass ejections (CMEs) — Sun: particle emission

1. INTRODUCTION

Solar energetic particles (SEPs) may give rise to major space weather hazards. The National Oceanic and Atmospheric Administration (NOAA) space weather scale for solar radiation storms characterizes the severity of the effects in three areas (biological, satellite operations, and other systems such as high-frequency communications) in accordance with the peak flux of >10 MeV ions[1]. For the practical purpose of preparing for possible space weather impacts, it is important to predict whether a SEP event will occur, when it will start, how intense it will become, and how long the SEP flux will stay above a given threshold. Even though a number of schemes have been proposed for SEP forecasting (e.g., Anastasiadis et al. 2017, and references therein), we still cannot reliably predict SEP events even after the possibly associated solar activity phenomenon is observed. This is obviously because our science-based understanding of the origins of SEP events is far from sufficient.

We often classify SEP events into two groups, impulsive and gradual (see Reames 1999, 2013) on the basis of their observed properties, including timescales, spectra, composition and charge states, and the associated radio bursts. In this scheme, it is the gradual SEP events with high ion (mostly proton) fluxes that can cause hazardous space weather conditions. Their close association with coronal mass ejections (CMEs)—as shown, for example, by Kahler et al. (1978, 1984) indicates that shock waves driven by energetic CMEs are responsible for energizing the ions in gradual SEP events, typically through diffusive shock acceleration (Lee et al. 2012; Desai & Giacalone 2016).

---

[1] https://www.swpc.noaa.gov/noaa-scales-explanation

Before the discovery of CMEs in the early 1970s, solar flares were thought to play a central role in causing coronal and interplanetary disturbances including protons observed in situ (e.g., Lin & Hudson 1976; Gosling 1993). However, in the two-class paradigm (Reames 1999, 2013), solar flares powered by magnetic reconnection are relevant primarily to impulsive SEP events that are typically enhanced in ^{3}He and heavy ions such as Fe, as compared with the elemental composition of the solar wind. Such compositional anomalies are hard to explain if the solar wind particles are accelerated by shock waves, as this requires some stochastic processes that can change the composition (see, for example, Miller et al. 1997).

There has been renewed interest in the role of solar flares in producing large gradual SEP events. This is due to the intimate association of gradual SEP events with type III radio bursts (which have been considered "flare" attributes, see Cane et al. 2002) and to the apparent correlations between SEPs and flare parameters (Dierckxsens et al. 2015; Grechnev et al. 2015; Trottet et al. 2015). However, these arguments may not exclude CMEs as the main contributor for gradual SEP events for the following reasons. First, CMEs are also frequently accompanied by type III bursts. Second, the parameters of large flares may vary in proportion to CME parameters as a result of the so-called "big-flare syndrome" (Kahler 1982). Moreover, there are no SEPs from intense flares if they are not associated with CMEs (e.g., all the X-class flares in AR 12192 in October 2014, see Sun et al. 2015), and some of the most intense SEP events can be associated with flares that are quite modest (Cliver 2016).

Therefore, we assume that particles in gradual SEP events, at least the large ones, are accelerated by CME-driven shock waves. In this assumption, we may expect a correlation between the SEP peak flux and the CME speed, which is generally the case, although for a given CME speed, a scatter of up to four orders of magnitude in the SEP peak fluxes was found (Kahler 2001). This large scatter can be attributed to a number of factors, ranging from the conditions for particle acceleration at the CME-driven shocks to the transport processes undergone by the particles. Earlier events may set up preconditioning in favor of SEP production by providing seed particles and producing enhanced levels of turbulence at the shock (e.g., Li & Zank 2005). Observationally, a CME preceded by another CME within a short interval tends to be more SEP-productive (Gopalswamy et al. 2004; Kahler & Vourlidas 2005). Additionally, even though the CME speed is a good measure of the shock speed, the efficiency of particle acceleration depends on various shock parameters that may vary significantly over the shock surface. The SEP flux may be affected by where on the shock the observer is dynamically connected to (e.g., Kouloumvakos et al. 2019, and refferences therein). These factors, together with the transport effects, that might involve cross-field diffusion (e.g., Zhang et al. 2009), affect not only the measured SEP peak but also the SEP temporal variations. The latter may often be consistent with the patterns expected from the longitude of the source region relative to the observer (Cane et al. 1988), but occasionally SEP events with prompt onsets may be observed even from poorly connected longitudes (e.g., Cliver 1982; Gómez-Herrero et al. 2015). It is likely that the observed SEP peak fluxes and temporal variations result from a combination of the above-mentioned factors. With this in mind, it is meaningful to study SEP events statistically in relation to the CME speed and the longitude of the source region.

In this paper, we present a statistical study of SEP occurrences and timescales with respect to CME source locations and speeds. Here we start from fast and wide CMEs and relate them to SEP properties. Most previous studies have started from SEP events and have then studied the properties of the associated CMEs and flares, ignoring CMEs not associated with SEP events. The recent study of 11 CMEs which did not produce SEP events by Lario et al. (2020) may be an exception. Our work focuses on the presence/absence and timescales of SEP events in association with individual CMEs, as presented in Sections 3 and 4, respectively. These are preceded by a description of our event list (Section 2) and followed by a discussion of how to explain our findings (Section 5). We summarize our conclusions in Section 6.

2. EVENT LIST

Our ultimate goal is to understand how the properties of CMEs may affect the properties of SEP events, such as their occurrence, peak fluxes and timescales. To acknowledge the fact that some energetic CMEs, even from well-connected longitudes, produce no SEPs or that CMEs from poorly-connected regions produce SEP events that quickly rise to a peak, it is meaningful to study all those CMEs irrespective of their associated SEPs and then to investigate the reasons for the wide variety of SEP properties. This approach complements one that discusses the properties of only those CMEs that are associated with SEP events (e.g., Kahler 2001).

Our study is based on fast ($v_{CME} \geq 900$ km s^{-1}) and wide (angular width $\geq 60°$) CMEs. In the first approximation, these CMEs may be considered to drive the shocks that are responsible for accelerating the protons observed at 1

AU, although the occurrence of a shock wave depends not only on the CME speed, but also on the conditions of the ambient solar wind. We imposed the restriction on angular width in order to exclude narrow CMEs, which are typically associated with small impulsive SEP events (Kahler et al. 2001). We selected them from the CDAW SOHO LASCO CME catalog[2] (Yashiro et al. 2004), which is a complete manually-generated catalog of CMEs as observed by the Large Angle and Spectrometric Coronagraph Experiment (LASCO: Brueckner et al. 1995) on board the Solar and Heliospheric Observatory (SOHO). Measurements of the kinematic parameters of CMEs included in the catalog come from visual inspection of all the available difference images.

Another important factor that can affect the properties of SEP events is the magnetic field connection between the observer and the CME-driven shock wave, which may be assumed to expand concentrically from the source region of the CME. If the region is on the visible side of the Sun, we can locate it using known low coronal signatures of CMEs, such as coronal dimming and post-eruption arcades (e.g., Zhang et al. 2007; Hudson & Cliver 2001; Nitta et al. 2014). These signatures are found in coronal images at extreme-ultraviolet (EUV) wavelengths. In order to maximize the number of CMEs for which source regions can be identified, including those from the far side, we have studied those CMEs that occurred since December 2006, so that we can make use of information from the EUV imagers on board the Solar-Terrestrial Relations Observatory (STEREO), in addition to those near the Sun-Earth line from SOHO (until 2010) and the Solar Dynamics Observatory (SDO: Pesnell et al. 2012, from 2010). All the fast and wide CMEs in solar cycle 24 were included in the period of our investigation (i.e., from December 2006 to October 2017). After examining the EUV images taken around the times of the 257 CMEs that meet our criteria for speed and angular width, we removed 18 CMEs for which source regions could not be identified. Almost all of them occurred while no STEREO data were available around the great conjunction in 2015.

Instead of discussing common SEP events observed by multiple spacecraft at separate longitudes (e.g., Richardson et al. 2014) or CMEs without SEPs at any of these spacecraft (Lario et al. 2020), we studied the SEP events (or lack thereof) at Earth, STEREO-A, and STEREO-B that are associated with each of the 239 CMEs. We thus have a total of 717 potential measurements. We extracted the time profiles of >10 MeV proton fluxes by using data with five-minute temporal resolution from the Energetic Particle Sensor (EPS: Onsager et al. 1996) on the Geostationary Operations Environmental Satellite (GOES) and from the High-Energy Telescope (HET: von Rosenvinge et al. 2008) and the Low-Energy Telescope (LET: Mewaldt et al. 2008), which belong to the suite of instruments for the In Situ Measurements of Particles and CME Transients (IMPACT: Luhmann et al. 2008) on STEREO. The >10 MeV integral flux is one of the standard products of GOES, but for STEREO / IMPACT we had to compute it by combining the HET and LET data, as illustrated by Gopalswamy et al. (2016).

Now we show how the >10 MeV proton flux compares between GOES and STEREO. Rodriguez et al. (2017) performed a cross-calibration between GOES and STEREO using two SEP events that occurred in 2006 December while STEREO-A and STEREO-B were still located near Earth. They reported that the STEREO $10-100$ MeV flux were smaller than GOES: the first, the second, and the third quartile of STEREO-A (STEREO-B) to GOES ratios are 0.850 (0.874), 0.926 (0.948), and 1.017 (1.071), respectively. We carried out the same analysis for the >10 MeV integral flux and confirmed that the first, the second, and the third quartile are 0.841, 0.921, and 1.008 for STEREO-A, and 0.858, 0.935, and 1.042 for STEREO-B. The 5th and 95th percentiles of the ratios are 0.736 and 1.215 for STEREO-A, and 0.767 and 1.272 for STEREO-B. Therefore 90% of >10 MeV integral fluxes agree within 27%.

In Table 1, we list the selected CMEs. The first three columns show the onset date and time, the projected speed, and the angular width of the CME, taken from the CDAW SOHO LASCO CME catalog. Note that the CME onset time is calculated by extrapolating the height-time profile in the LASCO field of view to the solar surface (1 solar radius from the Sun center). The next two columns show the magnitude and location of the associated solar flare. The remaining columns show the quality and the peak proton flux, if it exceeded 1 particle flux unit (pfu: defined as particles s^{-1} sr^{-1} cm^{-2}), separately for GOES, STEREO-A, and STEREO-B. The "quality" is one of the following.

- Good (110 events): SEPs are detected unambiguously with the peak >10 MeV proton flux exceeding 1 pfu. It is >10 pfu in 69 events and ≤10 pfu in 41 events. They are sufficiently well-observed that we can compute all the timescales (see Section 4).

- Contaminated (26 events): The observed SEP onset is clearly associated with the CME, but the later, post-peak temporal variations are contaminated by another SEP event due to a later CME or an energetic storm particle

---

[2] https://cdaw.gsfc.nasa.gov/CME_list/
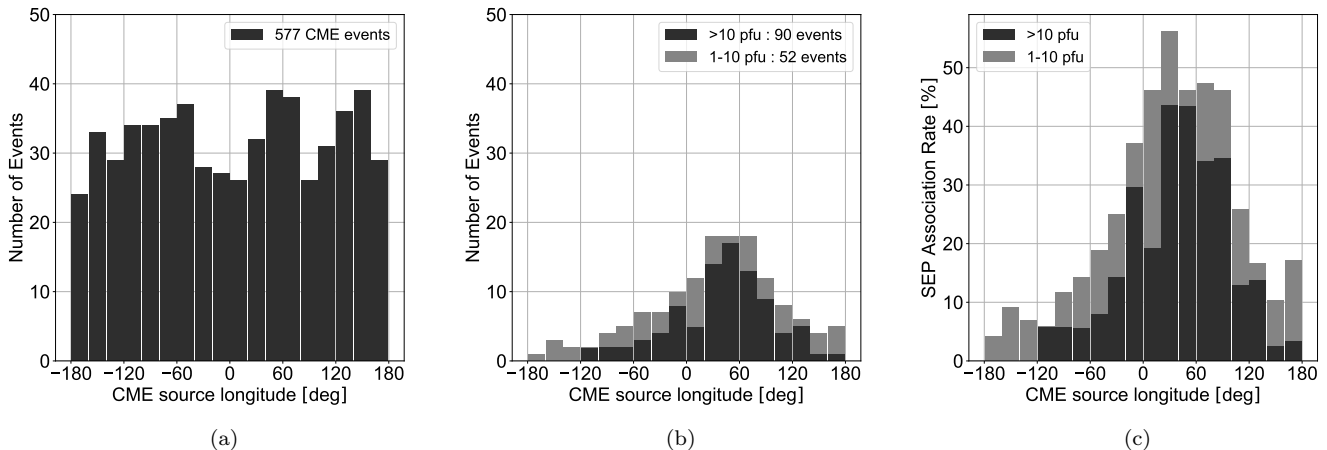
Figure 1. Distribution of CMEs with source longitude (in $20°$ bins) relative to the observer. (a) All the CMEs, irrespective of their associations with SEP events. CMEs that occurred during high background periods are excluded (39 HiB$\_N$ events, with $N \geq 10$, see Section 2). (b) Only the CMEs associated with a SEP event exceeding 10 pfu (black) and between 1 and 10 pfu (gray). (c) The percentage of CMEs associated with a SEP event (the color usage same as (b)). Panels (b) and (c) exclude 10 and 2 HiB$\_N$ events (with $N \geq 10$ and $N \geq 1$) for >10 pfu and $1-10$ pfu, respectively.

(ESP) event due to the shock wave driven by the present or an earlier CME[3]. In 15 events, the peak >10 MeV proton flux exceeds 10 pfu. We were able to measure all the timescales but the duration (see Section 4).

- No SEP (395 events): No >10 MeV protons are detected exceeding the 1 pfu level during the normal background. The normal background is about 0.2 pfu for GOES and about 0.1 pfu for STEREO-A and STEREO-B. In 71 of them, we noted a smaller enhancement (≤ 1 pfu), and they are so indicated.

- HiB$\_N$ (85 events): The background was elevated from the normal due to earlier events, preventing a small SEP event from being detected. Despite the higher background, however, we clearly find the presence of a SEP event in 18 cases, of which 16 have the peak >10 MeV proton flux that exceeds 10 pfu. An approximate background level (in pfu) is indicated by N. Subsets of these events, depending on N, are excluded in the discussion of the SEP association rate of CMEs (see Section 3).

- No data (79 events): No SEP data are available around the time of the CME. This includes the periods of no STEREO data due to the great conjunction in 2015, no STEREO-B data since its contact was lost in October 2014, and occasional data gaps for various reasons. These events are excluded in the following analysis.

- Multiple (22 events): No link can be established between the CME in question and the SEP event because of multiple CMEs and ESP events that occurred in succession. These events are excluded in the following analysis.

We note that the required threshold $v_{CME} \geq 900$ km s^{-1} excluded some large SEP events. Four >10 MeV proton events with peak fluxes exceeding 10 pfu are not included in this study. The starting dates of these events are 2012 July 12, 2013 April 11, 2014 November 1, and 2015 October 29. The speeds of their associated CMEs were 885 km s^{-1}, 861 km s^{-1}, 740 km s^{-1}, and 530 km s^{-1}, respectively. We also point out that our selected events are different from those in previous statistical studies of SEP events that were not restricted in CME parameters. For example, the fraction of CMEs with $v \geq 900$ km s^{-1} was only 147/217 and 85/214, respectively, in the works by Kahler (2013) and by Richardson et al. (2014). Accordingly, these authors included SEP events as observed by Wind, SOHO and STEREO that were too weak to be observed by GOES; since the GOES background is higher than those of the other three missions.

---

[3] There are a few confusing cases, where an ESP-related shock arrived during the SEP event in question. We identified a non-ESP peak before the shock arrival as the SEP peak.

(a) (b) (c)
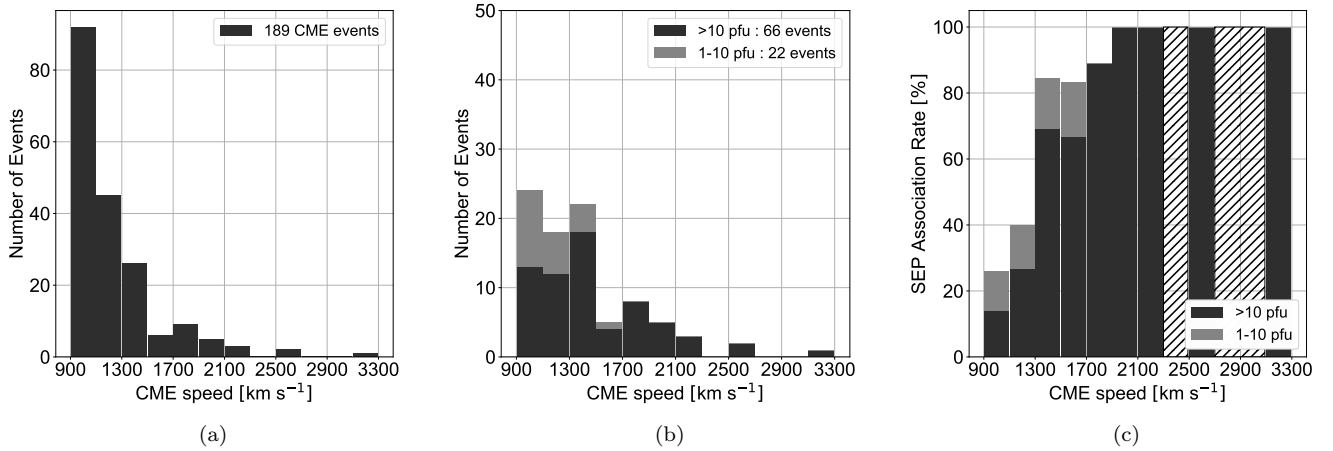
Figure 2. Distribution of CMEs with speed in 200 km s^{-1} bins. Here we limit the CMEs to those from the source longitudes E20–W100. (a) All the CMEs, irrespective of their associations with SEP events.(b) Only CMEs associated with a SEP event exceeding 10 pfu (black) and between 1 and 10 pfu (gray). (c) The percentage of CMEs associated with a SEP event (the color usage is the same as in (b)). Note that there were no CMEs between 2300 km s^{-1} and 2500 km s^{-1} and between 2700 km s^{-1} and 3100 km s^{-1}, as indicated by the hatched areas in panel (c). As in Figure 1, HiB_N events are excluded ($N \geq 10$ in (a), $N \geq 10$ and $N \geq 1$ in (b) and (c), for >10 pfu and 1–10 pfu, respectively.

3. SEP ASSOCIATION OF FAST AND WIDE CMES

This work involves careful analyses of EUV images to locate the region from which each of the selected CMEs originated, using known low coronal signatures of CMEs (e.g., Zhang et al. 2007; Hudson & Cliver 2001; Nitta et al. 2014). Figure 1 shows the distribution of our CMEs with the longitude of the source region relative to the observer. Note that the same CME can appear up to three times at different longitudes, as seen from Earth, STEREO-A, and STEREO-B. In Figure 1(a), we include all the CMEs, irrespective of their associations with SEP events, except for 39 "HiB_N" ($N \geq 10$) events (Section 2). In these high background events, the association with a SEP event exceeding 10 pfu is uncertain, since it is possible that such an event could be buried under the background. Thanks to multi-spacecraft observations, we have at least 23 CMEs in each of the 20° bins. Figure 1(b) shows the distribution of SEP-associated CMEs, and Figure 1(c) the ratio of SEP-associated CMEs to all CMEs. In Figures 1(b) and 1(c), we show the association of CMEs with SEP events as defined by two thresholds for the peak flux: 10 pfu and 1 pfu. Figure 1(c) shows that the SEP association rate is elevated in the range of longitude of E20–W100. We therefore refer to this range of longitude as "well-connected" in this section (i.e., Figures 2 and 4(a)). This is broader than what was shown in previous studies on the longitudinal distributions of SEP events (e.g., Smart & Shea 1996; Laurenza et al. 2009). It is possible that the broader distributions in Figure 1(c) may be characteristic of our SEP events measured at >10 MeV, most of which come from solar cycle 24.

In Figure 2, we show the distribution of CMEs with speed in 200 km s^{-1} bins. Here we limit the CMEs to those from the well-connected longitudes (E20–W100). As expected, there are more CMEs that are slower (but $\geq$ 900 km s^{-1}), although the SEP association rate rises sharply with the CME speed. All the CMEs faster than 2100 km s^{-1} are associated with a SEP event.

The dependence of the SEP association rate of CMEs on both the longitude of the source region and the CME speed can be visualized in heat maps, as shown in Figure 3. Here the maps come from a 2D array of the longitude relative to the observer (in 45° bins) and the speed (in 600 km s^{-1} bins) of the CME. Colors from yellow to red represent low to high association rates, as indicated in the color bars in the figure. Note that the SEP association rates have large uncertainties except for the bottom row because of the limited number of events. Figures 3(a) and 3(b) are heat maps for the SEP association rate for SEP events with threshold peak fluxes >10 pfu and >100 pfu, respectively. The number of all the CMEs and of the SEP-associated CMEs, together with the association rate, is also indicated in each cell. As in the previous figures, we exclude the HiB_N events that prevent us from determining the association of the CME with a SEP event. For the association with SEP events exceeding 10 pfu (panel (a)), 39 events with $N \geq 10$
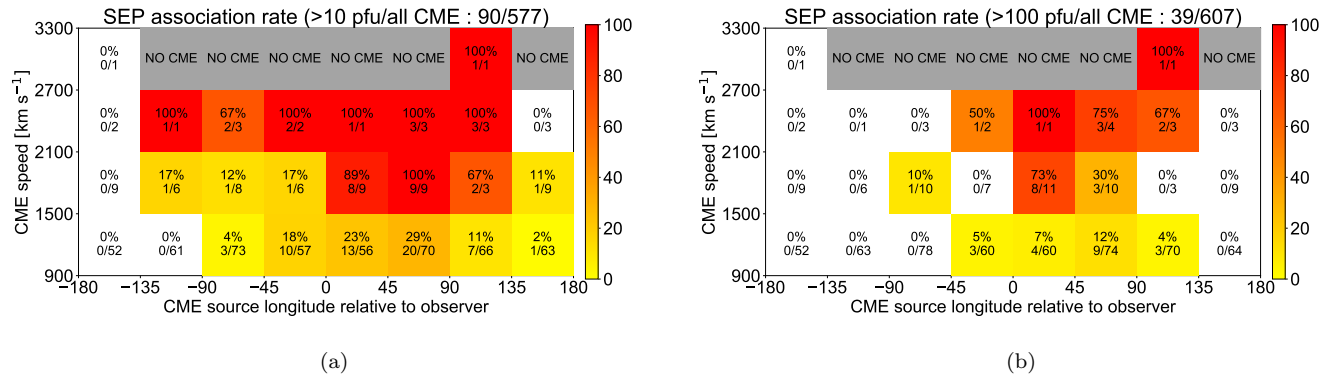
Figure 3. SEP heat maps, showing how the SEP association rate varies with the source longitude and speed of the CME. (a) and (b) show, respectively, a heat map for SEP events >10 pfu and >100 pfu. Higher (lower) association rates are shown in red (yellow). Cells in gray indicate no CMEs in those ranges of speed and source longitude. Cells in white indicate no SEP association. Different numbers of the HiB_N events are excluded in (a) and (b), depending on N; $N \geq 10$ and $N \geq 100$ for (a) and (b), respectively (see text).

are excluded. For SEP event exceeding 100 pfu (panel (b)), 9 events with $N \geq 100$ are excluded. As a result, the number of all the CMEs is greater in panel (b). Note that there was only one CME faster than 2700 km s^{-1}, which occurred on 2017 September 10. Its speed was 3163 km s^{-1}. This CME appears twice in each heat map, since it occurred after the contact with STEREO-B was lost. Its source location was S09W90 from Earth. This translates to E142 from STEREO-A, at which only a weak SEP event was observed that seemed to be directly linked to the CME. The >10 MeV proton flux peaked on September 12[4], and the peak flux was less than 10 pfu. Therefore the top left cell indicates no SEPs in Figures 3(a) and 3(b). There were fewer CMEs with higher speeds, and based on limited statistics, it appears that faster CMEs are associated with SEPs over wider longitudes. For the association rates of CMEs with SEP events for which the peak exceeded 10 pfu, we can confirm that faster CMEs contribute more to the SEP association rate. For example, Figure 1(c) shows that the SEP association rate of CMEs around W60 is ~40%, which results from the 100% association rate for CMEs faster than 1500 km s^{-1} offsetting the lower association rate for slower CMEs. Figure 3(b) shows that the CMEs associated with >100 pfu SEP events not only are much rarer but also are limited to higher speeds and narrower ranges of longitude.

In space weather applications, the SEP peak flux is routinely forecast using basic properties of CMEs and flares. In Figure 4, we show the relations among the SEP peak flux, the CME speed, and the magnitude of the associated flare. Figure 4(a) shows the relation between the peak proton flux and the CME speed. Even though they appear to be weakly correlated, especially for those events in the well-connected longitudes (plotted in blue), there is considerable scatter, as found in past studies (e.g., Kahler 2001); the peak proton flux for the same CME speed can vary by three orders of magnitude, even though we limit the CMEs to fast ones ($v_{CME} \geq 900$ km s^{-1}) in this study. This is unlike Kahler (2001), who included even CMEs slower than 200 km s^{-1}. The regression lines of each group of longitudes are also shown in Figure 4(a). The peak proton flux tends to be higher for the SEP events from well-connected longitudes. The difference is about one order of magnitude for a CME with 2000 km s^{-1}.

In Figure 4(b), we plot the peak soft X-ray (SXR) flux of the associated flare vs the CME speed, considering separately those CMEs associated with, and not associated with, >10 pfu protons. There is a somewhat higher correlation for SEP-associated CMEs, which tend to be faster (Figure 2(a)). This relation may largely reflect the big-flare syndrome (Kahler 1982). Figure 4(c) shows a weak correlation between the peak SXR flux and peak proton flux, irrespective of whether the source region is in the western or eastern hemisphere. Note that this plot contains only flares that were associated with fast and wide CMEs. The scatter would be much more pronounced if all flares were included irrespective of their associations with CMEs.

4. SEP TIMESCALES

[4] A higher (>100 pfu) >10 MeV proton flux was seen on September 14, but this appears to have been due to a stream interaction region rather than to the CME on September 10 (see Guo et al. 2018).
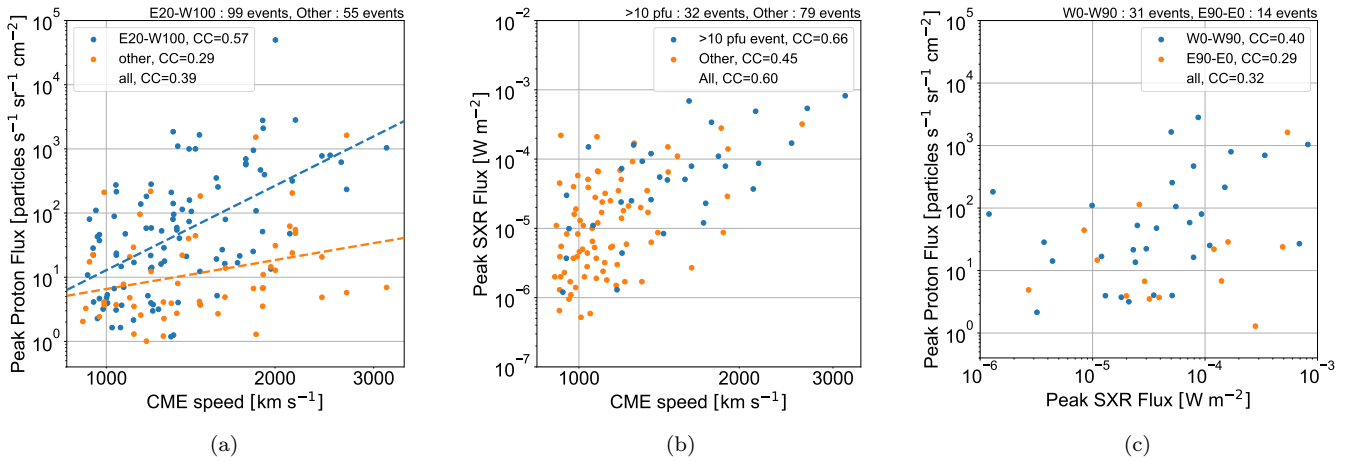
Figure 4. (a) Correlation between CME speed and peak proton flux. Each symbol shows whether or not the events come from well-connected longitudes. The dashed lines are the regression lines for each group. All the events in which the peak proton flux was measured are included ("Good", "Contaminated", and "HiB_N"). (b) Soft X-ray (SXR) flux vs CME speed as observed by GOES. This figure contains only the data from frontside events at longitudes E90-W90 from GOES. The symbols show whether or not each CME is associated with a >10 pfu SEP event. (c) Peak proton flux vs soft X-ray flux (both from GOES) for frontside events.

The timescales are also important properties of SEP events. Typical questions include: When does the SEP event start? How fast does it rise to the peak? And how long does it stay at a high level? We measured the key times of SEP events only when the onset was clearly found. They are labeled either "Good" or "Contaminated" in Table 1, not including events that have high pre-event background. If the quality in Table 1 is "Good"— we measured the following four times in this study: the SEP start time, the SEP half-peak (start), the SEP peak time, and the SEP half-peak (end). We measured all times on a log scale plot. We defined the SEP start time manually as the time when the proton flux increased above the background, typically in three consecutive 5 min intervals. The SEP peak time is usually the time after the SEP start time when the proton flux is the highest. More complex cases are described below. The SEP half-peak (start) and SEP half-peak (end), respectively, were automatically extracted as the times when the proton flux first exceeded—and last went below—half of the flux at the SEP peak time.

Many SEP events show simple rise-and-fall time profiles, and we were able to measure the four times defined above unambiguously for these events. However, in some events the proton flux time profile exhibited a second or even third peak, following a plateau or plateaus after the first peak. In such events, we usually took the time of the first peak as the SEP peak time. This is because later peaks may be produced by transport effects and thus may not directly reflect the CME properties. Other SEP events show a clear onset, but subsequent time profiles are contaminated either by another SEP event due to a later CME or by an ESP event locally produced by the passage of the shock wave driven by the present or an earlier CME. They are labeled "Contaminated" in Table 1. We did not measure the SEP half-peak (end) for any of these 26 events, but in all of them the SEP peak was clearly seen, allowing us to measure the SEP start time, SEP half-peak (start) and SEP peak time.

From these times, we calculated the four timescales listed in Table 2. They are illustrated in Figure 5 using an example of a real SEP event. Here, TO is the onset time, which measures how quickly the SEP event starts at 1 AU (defined as the SEP start time) after the CME launch at 1 $R_\odot$; TR is the rise time from the SEP start time to the SEP half-peak (start); Tm is the full rise time from the SEP start time to the SEP peak time; and TD is the duration, i.e., the length of time during which the proton flux stays above half the peak value, which is between SEP half-peak (start) and SEP half-peak (end). These notations—TO, TR, and TD—were adopted by Kahler (2013). He also used OR, which is the sum of TO and TR; that is, the time from the CME launch at 1 $R_\odot$ to SEP half peak (start). The timescale Tm is a redefinition of ΔT_m that was first used by Van Hollebeke et al. (1975).

Here we study the correlation of the SEP timescales TO, TR and TD with CME source longitude and speed. The plots in Figure 6 show the correlation of TO and TR with the CME source longitude relative to the footpoint of the Parker spiral ($\Delta\Phi$). We calculated the longitude on the solar surface of the nominal footpoint of the Parker spiral
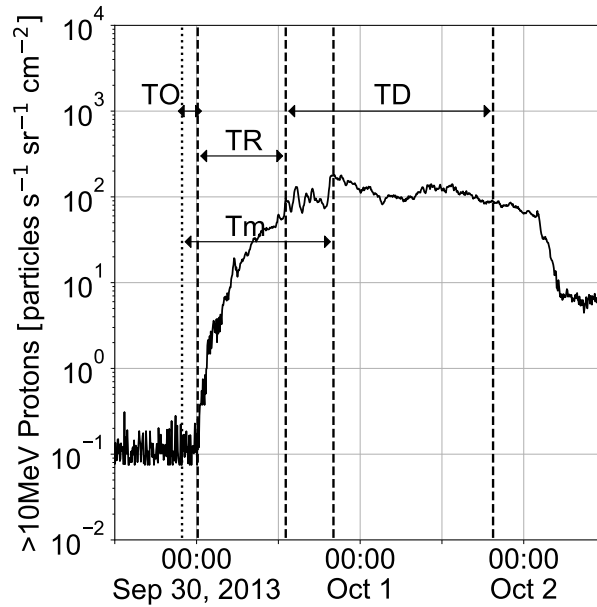
Figure 5. An example showing the four timescales defined in the text. The dashed lines, from left to right, are the SEP start time, the SEP half-peak time (start), the SEP peak time, and the SEP half-peak time (end). The dotted line is the CME launch time from SOHO LASCO CME catalog.

that was connected to GOES, STEREO-A, and STEREO-B, using the solar wind speed around the time of the SEP onset, as sampled by Wind and STEREO. When the Wind data were missing, we used data from the Advanced Compositional Explorer (ACE). Some events had to be dropped because we were not able to calculate the longitude of the Parker spiral footpoint due to the unavailability of solar wind data. These timescales are plotted vs $\Delta\Phi$ in Figures 6(a–c), where larger and darker circles indicate faster CMEs. Figure 6(a) shows that CMEs from regions within 60° in longitude from the footpoint of the Parker spiral tend to be associated with SEPs with short onset times. In this region of $\Delta\Phi$, TO is almost always shorter than five hours but longer than one hour. Note that it takes 1.15 hours for 10 MeV protons to travel the distance of 1.2 AU, which is often used as a typical path length for the Parker spiral corresponding to a solar wind speed of $\sim$400 km s^{-1}. The longest TO is about 18 hours for an event that is far outside this range of $\Delta\Phi$. In Figure 6(b), we find a similar trend for TR with $\Delta\Phi$, but with more scatter, even for $|\Delta\Phi| < 60°$. In Figure 6(c), TD is characterized by a broad distribution for most ranges of $\Delta\Phi$, with occasional high values.

Next we consider how TO, TR, and TD depend on the CME speed (v_{CME}), as plotted in Figures 7, 8, and 9, respectively. Panel (a) in each of these figures plots individual data, color coded to distinguish five ranges of the relative longitude as indicated in the legends. We produced panel (b) by grouping all the events into five longitudinal ranges, sorting each group into four subgroups by v_{CME}, and finally taking the average in each of the four v_{CME} subgroups. This analysis follows the work by Kahler (2013), and it is intended to make statistical trends easier to discern. We adjusted the ranges of v_{CME} in the four subgroups in each longitude range so that each subgroup contains roughly the same number of events. In Figure 9, we note a reduced number of events that belong to each of the five longitudinal groups. This is because for a number of events the SEP half-peak (end) could not be measured, and therefore TD could not be calculated. According to Figures 7–9, the correlations of the timescales with v_{CME} are not strong. The apparent correlations are susceptible to grouping of the events in different longitude ranges, and taking medians instead of averages does not make the correlations any more solid. Nevertheless, we do see positive correlations for TR and TD with v_{CME}, especially for poorly connected (large $|\Delta\Phi|$) events. Furthermore, TO appears to be negatively correlated for small $|\Delta\Phi|$ events. These trends are consistent with previous results (e.g., Pan et al.
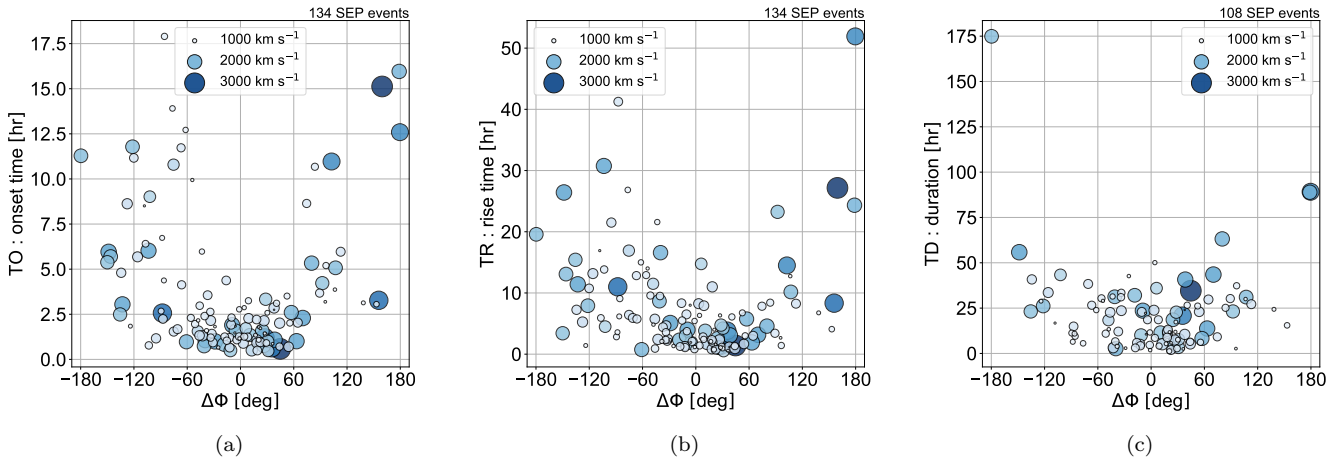
Figure 6. (a) SEP onset time from the CME launch (TO) vs the longitude of the CME source region relative to the footpoint of the Parker spiral. (b) and (c) The same plot, but for the SEP rise time TR and SEP duration TD. The size and darkness of the circles correspond to the CME speed. Almost all the SEP events listed in Table 2 are included in panel (a) and (b), except for the one on 2006 December 13 observed at STEREO-A and STEREO-B. This is because both STEREO were located near Earth and their data points are consistent with that of GOES. Events in the Contaminated category are excluded in panel (c) because TD cannot be measured.

2011; Kahler 2013). Finally, the relationship between TO and peak proton flux is shown in Figure 10. TO is the only timescale that shows a correlation with the peak proton flux. The correlation is rather strong especially near the footpoint of the Parker spiral. This trend was reported by Kahler (2013).

5. DISCUSSION

In order to clarify further the roles of CME-driven shocks in generating SEP events, we have carried out a statistical study of the SEP occurrences, peak fluxes, and timescales with respect to the CME source locations and speeds. As noted in Section 1, there are several other factors that could affect the SEP properties, such as preconditioning by earlier events (e.g., Li & Zank 2005, and references therein), spatial distributions of shock parameters closely related to particle acceleration and their time-dependent connections to the observer (e.g., Kouloumvakos et al. 2019, and references therein), transport effects (e.g., Zhang et al. 2009, and references therein), etc. How these factors as a whole affect the SEP properties can ideally be studied in individual events with a comprehensive approach that involves both data analyses and numerical simulations. On the other hand, it is also important to know the trend of how the SEP properties vary with respect to the CME source locations and speeds, as found in a large sample of events. Our approach of starting from CMEs, rather than from SEP events, complements other works that discuss the properties only of CMEs that are associated with SEP events. Recently, Lario et al. (2020) found 11 fast and wide CMEs that did not produce SEP events at any of the three locations, Earth, STEREO-A, or STEREO-B. They discussed these events in terms of a deficit in the release of particles at the time of the eruption and the limited extent of the strongest regions of the shocks driven by the CMEs. In this paper, we presented the statistical trends found in a large number of events observed at GOES, STEREO-A and STEREO-B. Moreover, we analyzed mostly solar cycle 24 events, whereas similar statistical studies dealt with solar cycle 23 events (e.g., Kahler 2005, 2013; Pan et al. 2011) or partially included solar cycle 24 events (e.g., Papaioannou et al. 2016). Another difference from previous studies of SEP timescales is that we used the CME source longitude relative to the footpoint of the Parker spiral ($\Delta\Phi$) rather than to the observer. We noted that $\Delta\Phi$ has been used previously for discussing SEP intensities in multi-spacecraft observations (e.g., Richardson et al. 2014).

We found the source regions of 239 fast ($v_{CME} \geq 900$ km s^{-1}) and wide (angular width $\geq 60°$) CMEs. Thanks to STEREO data, we were able to determine the CME source regions accurately, even on the far side of the Sun from the Earth, which was not possible for the solar cycle 23 events. We looked for SEPs at each location, and we calculated the SEP association rate with respect to the CME source longitude relative to the observer (Figures 1(c) and 3). We discussed only >10 MeV protons here, partly because they define the space weather effects characterized by NOAA.
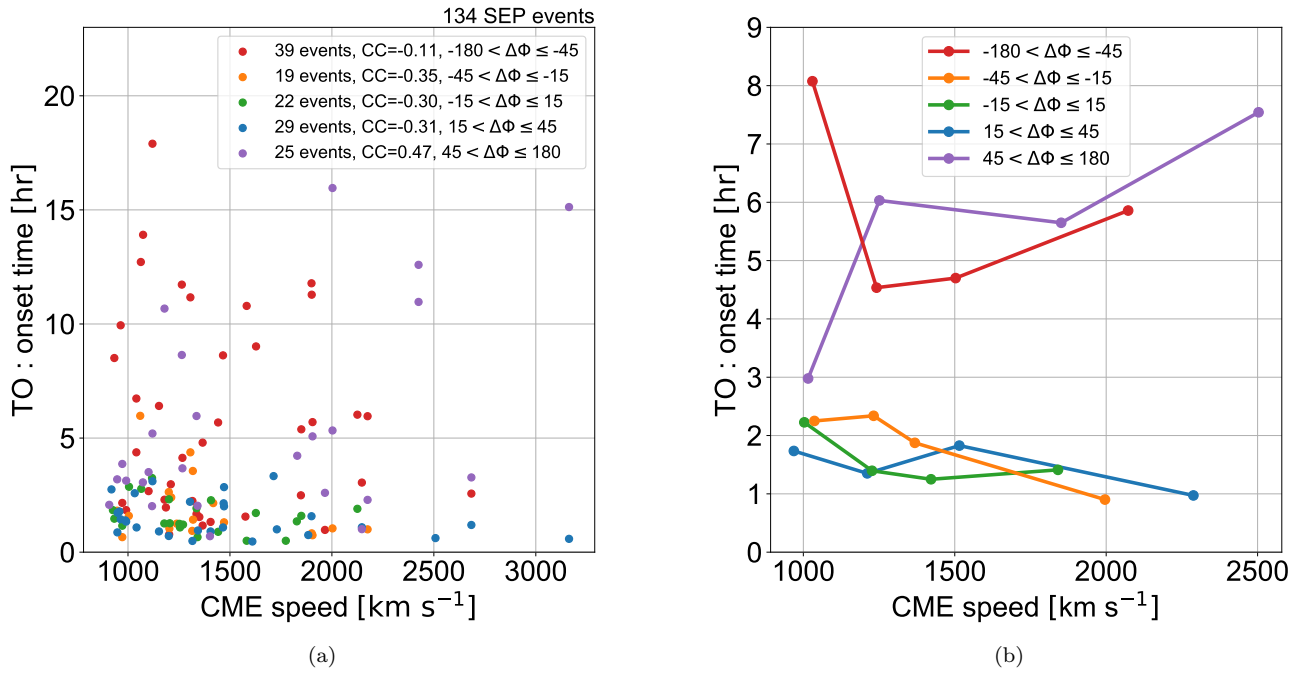
Figure 7. SEP onset time TO vs CME speed (v_{CME}). Different colors are used for events in different ranges of longitude relative to the footpoint of the Parker spiral. Individual TO values are plotted in the left panel. In the right panel, averaged TO values are plotted after re-grouping all the data into four representative CME speeds. The number of data points is the same as in Figure 6(a).
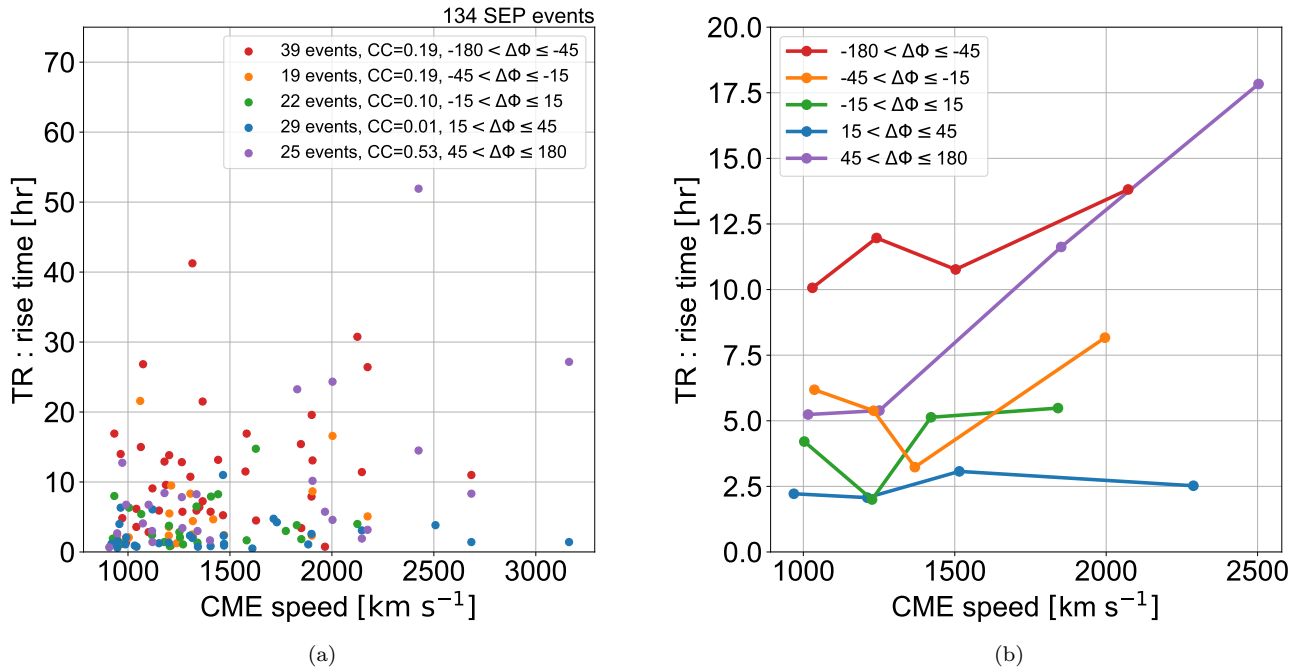
Figure 8. Same as Figure 7, but for the rise time TR. The number of data points is the same as in Figure 6(b).
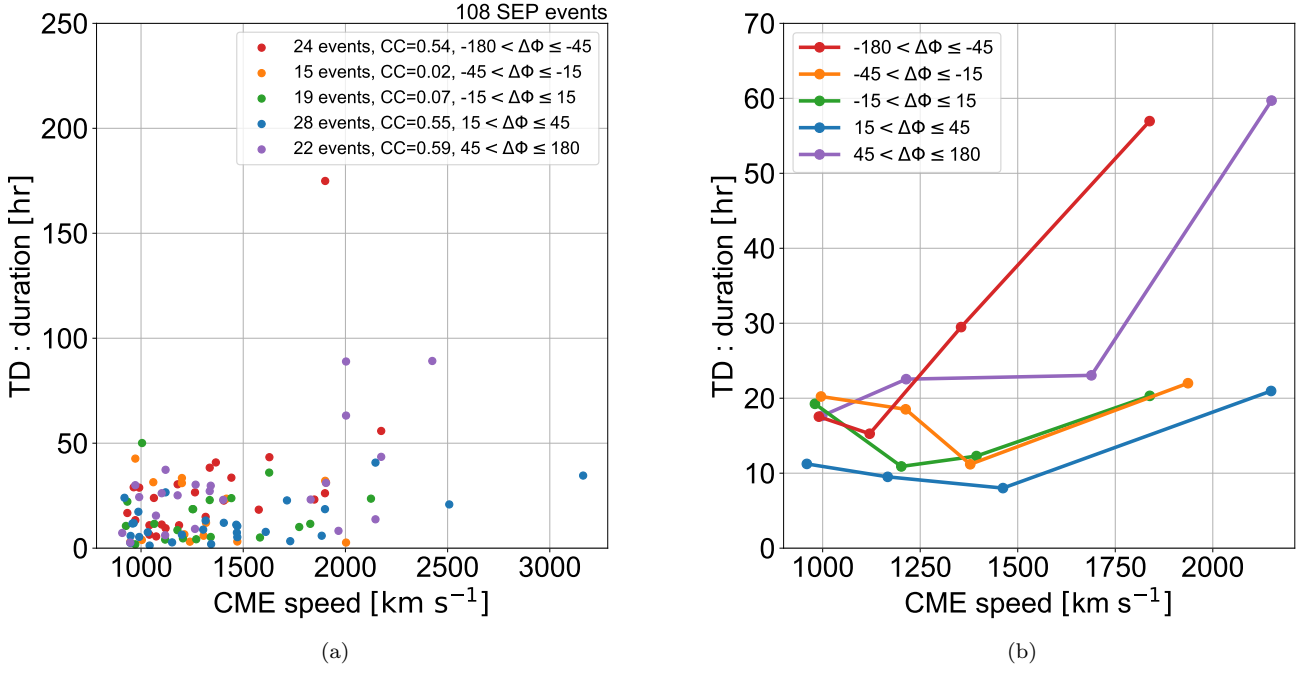
Figure 9. Same as Figure 7, but for the duration TD. The number of data points is the same as in Figure 6(c).
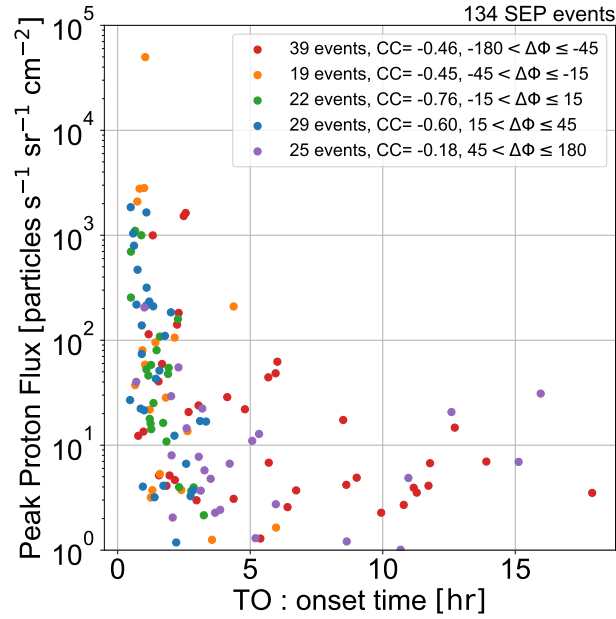
Figure 10. SEP onset time TO vs peak proton flux. The color and used data are same as Figure 7(a). The correlation coefficients are calculated between TO and logarithm of peak proton flux.

We found higher SEP association rates for CMEs that originate in what we usually consider to be well-connected longitudes. This suggests that the acceleration of >10 MeV protons is more efficient at the nose of a CME-driven shock than elsewhere, which also has been suggested to be the case for higher-energy protons (Gopalswamy et al. 2013). On the other hand, the SEP association rate is non-zero over a wide range of longitudes, consistent with multi-spacecraft observations of SEP events (e.g., Richardson et al. 2014). For CMEs faster than 900 km s^{-1}, only the narrower range of longitudes E180-E135 may be SEP-free. In this work, we did not extensively study the effect of the CME width on SEP events except that we limited to CMEs that were wider than 60°. We, however, note that full halo CMEs that have angular width of 360° more often accompany an SEP event than other CMEs (93/136 vs 33/103), supporting the recent study by Lario et al. (2020) that CMEs without SEPs tend to be narrow.

At the other extreme, a CME from well-connected longitudes must be faster than 1900 km s^{-1} to be always associated with a SEP event (Figure 2(c)), suggesting the importance of shock waves, even when the CME originates in this longitude range. Moreover, the peak proton flux from the regression line of well-connected events are one order of magnitude higher than that of poorly connected events with 2000 km s^{-1}, while the peak proton flux of well-connected events vary by three orders of magnitude (see Figure 4(a)). It implies that some important factors (e.g., preconditioning by earlier events) other than CME speed and source longitudes exist. Another factor that may account for the scatter of the peak SEP flux is the spatial extension of the CME-driven shock wave, which can vary for CMEs with similar speeds. This has recently been diagnosed using the bandwidth of hectometric type II bursts (Iwai et al. 2020).

By analyzing the timescales of SEP events, we found that TO (the SEP onset time relative to the CME launch) is correlated more tightly with $\Delta\Phi$ (the source longitude relative to the footpoint of the Parker spiral) than is TR (the SEP rise time) for $|\Delta\Phi| < 60°$ (Figure 6). The SEP onset is defined by the first-arriving particles. This finding seems to support the idea that only the first-arriving particles may be scatter-free. Particles that arrive later, even well before the peak, may undergo scattering, possibly by irregularities in the magnetic field, turbulence, etc., in the corona and interplanetary space. Past studies either showed no correlation (Kahler 2005; Pan et al. 2011) or a weak inverse correlation (Kahler 2013) between TO and v_{CME}. We followed Kahler (2013) in analyzing the grouping of v_{CME} into four subgroups and calculating median values—here we showed averages instead of medians. Our analysis also found weak inverse correlations between TO and v_{CME}, as shown by Kahler (2013) for the well-connected longitudes. Once protons are accelerated to >10 MeV, the strength of the shock, as approximated by the CME speed, may not affect the scatter-free transport of the first-arriving particles. As in previous works (Pan et al. 2011; Kahler 2013), we found a positive correlation of TR and TD with v_{CME} (Figures 8(b) and 9(b)). The positive correlation of TR and TD with v_{CME} may be explained if faster CMEs somehow produce wider areas over the shock surface that are favorable for particle acceleration. As a result. the observer would be connected to the regions that accelerate particles for longer time even though the magnetic field connection may change. We did not use Tm for our analysis because, as discussed by Pan et al. (2011), the full peak times do not necessarily represent typical peak times for each event, since proton time profiles often show multiple peaks. Moreover, though we did not show the graph, the tendency of Tm was similar to that of TR, so there is no problem in assuming that TR represents a typical peak time.

Concerning the question of how the timescales are related to the SEP flux, we found an inverse correlation between the peak proton flux and TO (but not TR or TD), similar to Kahler (2013), who pointed out that coarse time bin (half-hour) compromise the timing analysis and instead introduced a background effect to explain the apparent inverse correlation. We measured timescales in five-minute data, and found a strong negative correlation especially around the footpoint of the Parker spiral (Figure 10). This could be a consequence of the correlations between CME speed and TO, and CME speed and peak proton flux, but we may speculate that, in SEP events with shorter TO, the observer may connect to the CME-driven shock wave close to the Sun, while it is still strong and efficient in accelerating particles.

We found that the peak SEP flux appears to be correlated with the magnitude of the solar flare (Figure 4(c)). This does not necessarily mean that solar flares produce SEPs. All the flares included in the plot are associated with fast CMEs, and their magnitude is also weakly correlated with the CME speed (Figure 4(b)). It is well-established that there are no SEPs from intense flares if there are no CMEs (e.g., flares in AR 12192 in late October 2014; see Sun et al. 2015), and some of the most intense SEP events in solar cycle 23 were associated with flares that were quite modest (Cliver 2016). However, the GOES soft X-ray flux data are more readily available for space weather operations in real time. If combined with EUV imagery that shows low coronal signatures for CMEs—such as coronal dimming and post-eruption arcades—the information on solar flares may contribute to SEP forecasting. Another advantage of solar flares is that projection effects may not be as severe as for CMEs in estimating the speed. It is well known that the

true speed of a CME may differ from the projected speed, especially when it is launched far from the limb (Burkepile et al. 2004). In this study we used only the speed derived from LASCO observations, which may be an underestimate, especially for halo CMEs. In the future, we plan to compute the 3D speeds of CMEs, using the cone model (Xie et al. 2004) or the graduated cylindrical shell (GCS) model (Thernisien et al. 2006).

6. SUMMARY AND CONCLUSIONS

We conducted a statistical study of the SEP associations of all the fast and wide CMEs that occurred between December 2006 and October 2017. Our primary findings are summarized as follows:

1. The SEP association rate is higher for CMEs that come from the range of longitude of E20 – W100 relative to the observer.

2. A CME originating in a well-connected longitude needs to be faster than $\sim$2000 km s^{-1} to ensure 100% association with a SEP event.

3. The correlation of the peak SXR flux with the peak SEP flux is comparable to that of the CME speed only when the flare is associated with a fast and wide CME.

4. The SEP onset time tends to be short when the CME source region is close in longitude (within $\pm 60°$) to the footpoint of the Parker spiral. This trend is still present but weaker for the SEP rise time.

5. There are inverse correlations between the SEP onset timescale and the CME speed in events from regions close in longitude to the footpoint of the Parker spiral.

6. There are positive correlations of the SEP rise timescale and duration with the CME speed.

7. There are inverse correlations between the peak proton flux and onset timescale.

In addition to computing the de-projected velocities of CMEs using well-established models, our next steps may include studying proton spectra, associations with electron events and radio bursts, and detailed characterizations of eruptions in the low corona before they arrive at coronagraphic heights.

Table 1. Properties of Fast and Wide CMEs and Associated SEP Events

CME parameters					GOES		STEREO-A		STEREO-B	
launch	speed	width	Flare Class	Flare site	quality	Ip	quality	Ip	quality	Ip
date,time	(km/s)	(deg)				(pfu)		(pfu)		(pfu)
2006-12-13 02:25	1774	360	X3.4	S06W23	Good	698.0	Good	592.1	Good	567.4
2006-12-14 22:00	1042	360	X1.5	S06W46	Good	215.0	HiB_9	[23.6][a]	HiB_7	[22.1][a]
2007-01-25 06:33	1367	360	C6.3	S08E090	No SEP	—	No SEP	—	No SEP	—
2007-05-19 12:56	958	106	B9.5	N07W06	No SEP	—	No SEP[b]	—	No SEP[b]	—
2007-12-31 00:37	995	164	C8.3	S08E081	No SEP	—	No SEP	—	No SEP	—
2008-03-25 18:37	1103	112	M1.7	S13E078	No SEP	—	No SEP	—	No SEP	—
2010-02-12 22:13	1180	120	C3.0	N25W56	No SEP	—	No SEP	—	No SEP	—
2010-02-13 21:36	1005	63	—	N30W63	No SEP	—	No SEP	—	No SEP	—
2010-03-01 22:35	1518	87	—	N26E075	No SEP	—	No SEP	—	No SEP	—
2010-03-06 07:35	1009	127	B5.2	N25E15	No SEP	—	No SEP	—	No SEP	—
2010-03-13 16:45	1258	95	—	N31W73	No SEP	—	No SEP	—	No SEP	—
2010-08-14 09:49	1205	360	C4.4	N17W52	Good	14.2	No SEP[b]	—	No SEP[b]	—
2010-08-18 05:29	1471	184	C4.5	N17W101	Good	3.7	Good	3.7	No SEP[b]	—
2010-08-31 20:40	1304	360	—	S22W146	No SEP[b]	—	Good	1.2	No SEP	—
2011-02-24 07:16	1186	158	M3.5	N16E83	No SEP	—	No SEP	—	No SEP	—
2011-03-07 19:51	2125	360	M3.7	N30W48	Good	47.7	Contaminated	62.4	HiB_3	—
2011-03-19 12:03	1102	140	—	S25W109	No SEP	—	No SEP	—	HiB_3	—
2011-03-21 02:13	1341	360	—	N16W129	Good	8.0	Good	1102.9	No SEP	—
2011-03-29 20:14	1264	195	—	N20E117	No SEP	—	Good	1.2	Good	4.1
2011-04-04 13:48	2081	109	—	N20E133	No SEP[b]	—	No SEP	—	No SEP	—
2011-04-27 02:21	924	257	C2.0	N17E57	No SEP	—	No SEP	—	No SEP	—
2011-05-06 08:36	1024	169	—	N17E139	No SEP	—	No SEP	—	No SEP	—
2011-05-09 20:39	1318	292	C5.4	N18E93	No SEP[b]	—	No SEP	—	Good	1.3
2011-05-18 18:02	1105	126	C2.0	N09W95	No SEP	—	No SEP[b]	—	No SEP	—
2011-05-29 20:53	1407	186	C8.7	S19E72	No SEP	—	No SEP	—	No data	—
2011-06-02 07:43	976	360	C3.7	S19E25	No SEP	—	No SEP	—	No SEP[b]	—
2011-06-04 06:26	1407	360	—	N16W144	No SEP	—	Contaminated	159.2	No SEP	—
2011-06-04 21:47	2425	360	—	N16W153	Contaminated	4.9	HiB_90	[777.0][a]	Good	20.7
2011-06-07 06:15	1255	360	M2.5	S21W54	Good	52.7	HiB_50	—	HiB_6	—
2011-06-13 03:37	957	360	—	S19E135	HiB_4	—	No SEP	—	HiB_2	—
2011-07-09 16:10	991	90	—	N24W120	No SEP	—	No SEP	—	No SEP	—
2011-08-04 03:39	1315	360	M9.3	N19W36	Contaminated	80.1	No SEP[b]	—	No SEP[b]	—
2011-08-08 17:53	1343	237	M3.5	N16W61	Good	4.0	No SEP	—	No SEP	—
2011-08-08 22:49	1070	74	C5.3	N19W65	HiB_1	—	No SEP	—	No SEP	—
2011-08-09 03:24	1146	141	M2.5	N18W68	HiB_0.7	—	No SEP	—	No SEP	—
2011-08-09 07:52	1610	360	X6.9	N17W69	Good	26.9	No SEP	—	No SEP	—
2011-08-11 10:10	1160	167	C6.2	N15W97	No SEP	—	No data	—	No SEP	—
2011-09-07 18:23	924	188	—	N19E142	HiB_3	—	No SEP[b]	—	No SEP	—
2011-09-08 21:53	983	281	—	N19W147	No SEP	—	No SEP[b]	—	No SEP	—
2011-09-21 22:00	1007	255	—	N19W120	No SEP[b]	—	No SEP[b]	—	No SEP	—
2011-09-22 10:33	1905	360	X1.4	N09E89	Contaminated	6.8	Good	11.0	Good	2095.7
2011-09-24 09:27	1936	145	X1.9	N12E60	HiB_10	—	HiB_3	—	Multiple	—
2011-09-24 12:38	1915	360	M7.1	N10E56	HiB_10	—	HiB_2	—	HiB_100	[396.8][a]
2011-09-24 19:07	972	360	M3.0	N12E42	HiB_10	—	HiB_1	—	Multiple	—
2011-10-01 20:28	1238	360	—	N24E119	No SEP	—	No SEP	—	No SEP	—
2011-10-04 12:32	1101	360	—	N26E153	No SEP	—	Good	4.8	Good	20.7
2011-10-22 10:18	1005	360	M1.3	N25W77	Good	4.0	No SEP[b]	—	No SEP	—
2011-11-03 21:42	991	360	—	N09E154	Good	3.7	Good	210.5	Good	4.1
2011-11-09 12:57	907	360	M1.1	N24E35	No SEP	—	No SEP	—	No SEP[b]	—

Table 1 *(continued)*

CME parameters					GOES		STEREO-A		STEREO-B	
launch	speed	width	Flare Class	Flare site	quality	Ip	quality	Ip	quality	Ip
date,time	(km/s)	(deg)				(pfu)		(pfu)		(pfu)
2011-11-17 20:15	1041	360	—	N18E120	No SEP	—	No SEP[b]	—	Good	3.1
2011-11-26 06:52	933	360	C1.2	N17W49	Good	80.3	Good	17.4	No SEP[b]	—
2011-12-17 10:23	987	247	—	N26W121	No SEP	—	No SEP[b]	—	No SEP	—
2011-12-19 12:12	1092	154	—	S16W150	No SEP	—	No SEP	—	No SEP	—
2011-12-21 02:39	1064	360	—	S22E151	No SEP	—	No SEP	—	No SEP	—
2011-12-30 19:02	960	179	—	N54W158	No SEP	—	No SEP	—	No SEP	—
2012-01-02 14:45	1138	360	C2.4	N08W104	No SEP[b]	—	No SEP[b]	—	No SEP	—
2012-01-16 02:54	1060	360	C6.5	N34E86	No SEP	—	No SEP	—	Good	1.6
2012-01-19 14:41	1120	360	M3.2	N32E22	Good	3.5	No SEP	—	Good	17.0
2012-01-23 03:45	2175	360	M8.7	N28W21	Contaminated	2820.0	Good	48.4	Good	55.1
2012-01-26 04:41	1194	360	C6.4	N35W60	HiB_70	—	HiB_40	—	HiB_1	—
2012-01-27 18:18	2508	360	X1.7	N27W78	Good	796.0	Multiple	—	HiB_1	—
2012-02-25 14:36	1039	97	—	N19E93	HiB_2	—	No SEP[b]	—	No SEP	—
2012-03-03 18:13	1078	192	C1.9	N17E67	No SEP	—	No SEP	—	No SEP[b]	—
2012-03-04 10:40	1306	360	M2.0	N19E61	Contaminated	3.9	No SEP	—	Good	209.6
2012-03-05 03:31	1531	360	X1.1	N17E52	HiB_1	—	No SEP[b]	—	HiB_100	—
2012-03-07 00:16	2684	360	X5.4	N17E27	Contaminated	1630.0	Contaminated	5.8	Contaminated	233.7
2012-03-07 00:56	1825	360	X1.3	N15E26	Multiple	—	Multiple	—	Multiple	—
2012-03-09 03:43	950	360	M6.3	N15W03	HiB_500	—	HiB_4	—	HiB_80	—
2012-03-10 17:35	1296	360	M8.4	N17W24	HiB_100	—	HiB_20	—	HiB_10	—
2012-03-13 17:20	1884	360	M7.9	N17W66	Good	469.0	HiB_10	—	HiB_3	—
2012-03-18 00:04	1210	360	—	N18W116	No SEP	—	Contaminated	3.0	No SEP[b]	—
2012-03-21 07:12	1178	360	—	N18W160	No SEP	—	Good	58.1	No SEP	—
2012-03-23 23:58	1152	360	—	N18E164	No SEP	—	Good	138.3	Contaminated	2.6
2012-03-26 22:38	1390	360	—	N17E124	No SEP	—	No SEP	—	HiB_6	[21.1][a]
2012-03-27 02:46	1148	162	C5.3	N19W05	No SEP	—	No SEP	—	HiB_20	[95.9][a]
2012-03-28 01:24	1033	360	—	N21E116	No SEP	—	No SEP	—	HiB_50	[89.0][a]
2012-04-09 12:11	921	360	C3.9	N20W65	No SEP	—	No SEP	—	No SEP	—
2012-04-15 02:06	1220	173	C1.7	N10E90	No SEP	—	No SEP[b]	—	No SEP[b]	—
2012-04-16 00:07	1128	81	C1.8	N12E88	No SEP	—	No SEP	—	No SEP	—
2012-04-16 17:16	1348	166	M1.7	N14E88	No SEP	—	No SEP	—	No SEP	—
2012-04-30 07:19	992	135	C3.9	S18W88	No SEP	—	No SEP	—	No SEP	—
2012-05-17 01:25	1582	360	M5.1	N11W76	Good	255.0	Contaminated	2.7[c]	No SEP[b]	—
2012-05-26 20:29	1966	360	—	N15W121	Good	14.5	Contaminated	13.5	No SEP[b]	—
2012-06-02 04:12	1175	130	C1.5	N16E42	No SEP	—	No SEP	—	No SEP	—
2012-06-08 00:18	992	72	—	N16W42	No SEP	—	No SEP	—	No SEP	—
2012-06-14 13:39	987	360	M1.9	S17E06	No SEP[b]	—	No SEP	—	No SEP[b]	—
2012-06-23 06:57	1263	360	C2.7	N18W101	No SEP	—	No SEP	—	No SEP	—
2012-06-26 12:28	920	89	C1.3	N21E77	No SEP	—	No SEP	—	No SEP	—
2012-06-28 19:29	1313	145	C1.7	N18E48	No SEP	—	Multiple	—	No SEP[b]	—
2012-07-02 06:10	988	134	—	S09W58	No SEP	—	Multiple	—	Multiple	—
2012-07-02 08:03	1074	360	—	S16E134	No SEP	—	No SEP[b]	—	Good	7.0
2012-07-05 21:15	980	94	M1.6	S12W46	No SEP	—	No SEP	—	No SEP	—
2012-07-06 02:34	1059	73	M1.0	S12W48	No SEP	—	No SEP	—	No SEP	—
2012-07-06 22:54	1828	360	X1.1	S13W59	Good	25.2	No SEP[b]	—	No SEP	—
2012-07-08 16:08	1572	157	M6.9	S17W74	HiB_2	[19.2][a]	Multiple	—	No SEP	—
2012-07-09 05:32	1199	63	C4.6	S14W91	HiB_20	—	HiB_10	—	No SEP	—
2012-07-17 14:03	958	176	C9.9	S15W65	Good	110.0	No SEP	—	No SEP	—
2012-07-19 05:13	1631	360	M7.7	S13W88	HiB_20	[79.6][a]	HiB_1	[13.9][a]	No SEP	—
2012-07-23 02:15	2003	360	—	S17W132	Good	12.8	Good	49778.4	Good	31.0
2012-08-17 04:42	931	137	C1.8	N19E98	No SEP	—	No SEP	—	No SEP	—

Table 1 *(continued)*

CME parameters					GOES		STEREO-A		STEREO-B	
launch	speed	width	Flare Class	Flare site	quality	Ip	quality	Ip	quality	Ip
date,time	(km/s)	(deg)				(pfu)		(pfu)		(pfu)
2012-08-17 12:07	910	64	B7.8	N19E99	No SEP	—	No SEP	—	No SEP	—
2012-08-18 00:35	986	145	C1.4	N19E86	No SEP	—	No SEP	—	No SEP	—
2012-08-21 19:52	1024	360	—	S22E156	No SEP	—	HiB_1	[1.6][a]	No SEP	—
2012-08-31 19:44	1442	360	C8.4	S19E42	Good	44.3	No SEP	—	Good	999.9
2012-09-20 14:31	1202	360	—	S15E155	No SEP	—	HiB_10	[281.8][a]	Contaminated	12.3
2012-09-23 14:51	939	258	C1.7	S08E105	No SEP[b]	—	HiB_5	—	HiB_20	—
2012-09-27 09:57	1319	360	—	S25W151	No SEP	—	Contaminated	95.4	No SEP	—
2012-09-27 23:31	947	360	C3.7	N09W31	Good	28.4	Multiple	—	Good	22.3
2012-10-14 00:14	987	360	—	N13E137	No SEP	—	Good	3.2	No SEP[b]	—
2012-11-08 10:38	972	360	—	S14W160	Good	2.4	Good	37.3	No SEP	—
2012-11-21 03:45	920	360	—	N11W99	No SEP	—	No SEP	—	No SEP	—
2012-11-23 23:00	1186	360	—	N14W130	No SEP	—	Good	5.1	No SEP	—
2012-12-05 00:01	963	231	C1.7	N14E83	No SEP	—	No SEP	—	No SEP	—
2013-01-15 03:55	966	81	C1.1	S32W58	No SEP	—	No SEP	—	No SEP	—
2013-02-06 00:06	1867	271	C8.7	N22E19	No SEP[b]	—	No SEP[b]	—	No SEP[b]	—
2013-02-12 22:52	1050	165	B5.9	S32W58	No SEP	—	No SEP	—	No SEP	—
2013-02-26 09:31	987	360	—	N07W123	No SEP[b]	—	No SEP[b]	—	No SEP	—
2013-03-05 03:23	1316	360	—	N10E144	No SEP	—	Good	1849.9	Good	140.8
2013-03-12 10:14	1024	196	C2.0	N25E001	No SEP	—	No SEP	—	No SEP	—
2013-03-15 06:42	1063	360	M1.1	N11E012	Good	14.7	No SEP	—	No SEP[b]	—
2013-03-22 08:17	972	123	—	N28W126	No SEP	—	No SEP	—	No SEP	—
2013-04-21 07:10	919	360	—	N10W119	Good	3.3	No SEP	—	No SEP	—
2013-05-13 02:00	1270	360	X1.7	N11E90	No SEP	—	No SEP	—	Good	17.8
2013-05-13 15:47	1850	360	X2.8	N11E85	Contaminated	1.3	No SEP[b]	—	Contaminated	108.3
2013-05-14 01:03	2625	360	X3.2	N08E77	HiB_1	—	No SEP	—	HiB_300	[621.0][a]
2013-05-14 22:23	971	63	—	N25E101	HiB_1	—	No SEP	—	HiB_30	—
2013-05-15 01:27	1366	360	X1.2	N12E64	Good	22.0	No SEP	—	HiB_30	—
2013-05-16 07:08	951	63	—	N10E115	HiB_20	—	No SEP	—	HiB_2	—
2013-05-17 08:46	1345	360	M3.2	N12E57	HiB_20	—	No SEP	—	No SEP	—
2013-05-22 12:55	1466	360	M5.0	N15W70	Good	1650.0	Contaminated	4.2	No SEP[b]	—
2013-06-16 14:13	1104	96	—	S14E132	No SEP	—	No SEP	—	No SEP[b]	—
2013-06-21 02:53	1900	207	M2.9	S16E73	Good	6.7	No SEP[b]	—	Good	51.4
2013-06-28 01:25	1037	360	C4.4	S18W19	No SEP	—	No SEP	—	No SEP	—
2013-07-18 19:41	939	63	C2.3	S09E77	No SEP	—	No SEP	—	No SEP	—
2013-07-22 05:57	1004	360	—	N16W155	No SEP	—	Good	5.3	No SEP[b]	—
2013-08-17 19:00	1202	360	M1.4	S05W30	No SEP[b]	—	No SEP	—	No SEP	—
2013-08-30 02:04	949	360	C8.3	N15E46	No SEP	—	No SEP	—	Good	4.1
2013-09-24 20:18	919	360	B6.5	N26E70	No SEP	—	No SEP	—	No SEP[b]	—
2013-09-29 21:52	1179	360	C1.3	N17W29	Good	182.0	No SEP[b]	—	Good	1.0
2013-10-05 06:41	964	360	—	S22E118	No SEP	—	Good	42.9	Good	2.3
2013-10-11 07:05	1200	360	—	N21E103	No SEP	—	Good	218.5	Good	21.8
2013-10-25 14:41	1081	360	X2.1	S06E69	No SEP[b]	—	No SEP[b]	—	HiB_20	[47.4][a]
2013-10-28 04:16	1201	156	M5.1	N08W71	Contaminated	4.0	No SEP	—	No SEP	—
2013-10-28 13:44	1073	93	M2.8	N06W75	HiB_3	—	No SEP[b]	—	Good	7.8
2013-10-29 21:28	1001	360	X2.3	N05W89	HiB_3	[4.8][a]	No SEP	—	HiB_2	—
2013-11-04 04:38	1040	360	—	N03W165	No SEP	—	HiB_5	[273.7][a]	HiB_5	—
2013-11-06 23:25	1033	360	M1.8	S11W97	Good	6.7	HiB_5	—	HiB_1	—
2013-11-07 10:03	1405	360	—	N02E151	HiB_3	—	Good	73.9	Good	997.5
2013-12-07 07:11	1085	360	M1.2	S16W49	No SEP	—	No data	—	No SEP	—
2013-12-12 03:08	1002	276	C4.6	S23W46	No SEP[b]	—	No SEP	—	No SEP	—
2013-12-23 07:58	1409	94	—	N25W103	No SEP	—	No SEP	—	No SEP	—

Table 1 *(continued)*

CME parameters					GOES		STEREO-A		STEREO-B	
launch	speed	width	Flare Class	Flare site	quality	Ip	quality	Ip	quality	Ip
date,time	(km/s)	(deg)				(pfu)		(pfu)		(pfu)
2013-12-26 02:41	1022	171	—	S27E137	Multiple	—	Multiple	—	Multiple	—
2013-12-26 03:02	1336	360	—	S09E166	Good	2.7	Good	54.6	Good	59.4
2013-12-28 17:09	1118	360	—	S15W125	Good	29.3	HiB_1	—	HiB_8	—
2013-12-31 10:15	1101	230	C8.8	S09E101	No SEP	—	No SEP	—	No SEP[b]	—
2014-01-04 19:00	977	360	M4.0	S11E34	No SEP[b]	—	No SEP	—	No SEP	—
2014-01-06 07:33	1402	360	—	S15W112	Good	40.1	No data	—	No SEP[b]	—
2014-01-06 09:58	957	76	—	S15E112	HiB_20	—	No data	—	No SEP[b]	—
2014-01-07 18:04	1830	360	X1.2	S15W11	HiB_10	[951.0][a]	No data	—	Good	6.7
2014-01-21 18:16	1035	113	—	S16W115	No SEP	—	Multiple	—	Multiple	—
2014-01-21 20:41	1065	221	—	S13E162	No SEP	—	Good	3.7	Multiple	—
2014-01-24 07:11	973	173	—	S14E130	No SEP	—	No SEP	—	No SEP	—
2014-01-26 08:03	1088	255	C1.5	S16E106	No SEP	—	No SEP	—	No SEP	—
2014-01-30 15:47	1087	360	M6.6	S13E58	No SEP	—	No SEP	—	No SEP[b]	—
2014-02-09 15:38	908	360	M1.0	S15E103	No SEP	—	Good	2.0	No SEP	—
2014-02-14 08:05	1165	360	—	S13W142	No SEP	—	No SEP	—	No SEP	—
2014-02-20 02:33	993	360	—	S17E143	HiB_3	—	No SEP	—	No SEP	—
2014-02-20 07:28	948	360	M3.0	S15W73	Good	22.3	No SEP	—	No SEP	—
2014-02-21 15:28	1252	360	—	S15E121	No SEP	—	No SEP[b]	—	Good	16.1
2014-02-22 12:04	1023	233	—	S34W145	No SEP	—	HiB_1	—	HiB_10	—
2014-02-25 00:32	2147	360	X4.9	S12E82	Contaminated	23.9	Good	205.2	Good	316.7
2014-03-04 21:16	911	86	—	N09E57	HiB_1	—	HiB_3	—	No SEP[b]	—
2014-03-12 14:08	972	360	—	N18E158	No SEP	—	Good	46.1	Good	4.7
2014-04-02 13:22	1471	360	M6.5	N11E53	No SEP	—	No SEP	—	Good	184.4
2014-04-02 23:13	1367	64	—	N14E152	No SEP	—	No SEP	—	HiB_50	—
2014-04-03 06:38	1156	71	C5.5	N10E50	No SEP	—	No SEP	—	HiB_20	—
2014-04-12 06:59	1016	139	C5.0	S12E86	No SEP	—	No SEP	—	No SEP	—
2014-04-18 12:43	1203	360	M7.3	S20W34	Contaminated	58.5	No SEP	—	No SEP	—
2014-05-05 14:57	1069	124	—	N04E102	No SEP	—	No SEP	—	No SEP	—
2014-05-07 15:44	923	360	M1.2	S11W100	No SEP[b]	—	No SEP	—	No SEP	—
2014-05-09 01:53	1099	360	—	S11W122	No SEP	—	No SEP	—	No SEP	—
2014-05-10 04:06	1086	360	—	S11W136	No SEP	—	No SEP[b]	—	No SEP	—
2014-06-06 13:28	1200	360	—	S19E132	No SEP	—	No SEP[b]	—	No SEP[b]	—
2014-06-10 11:29	925	111	X2.2	S15E80	No SEP	—	Multiple	—	Multiple	—
2014-06-10 12:44	1469	360	X1.5	S17E82	No SEP	—	Multiple	—	Good	12.3
2014-06-15 12:42	958	190	M1.1	S21W92	No SEP	—	No SEP	—	No SEP	—
2014-06-16 01:24	1088	69	C8.3	S14W107	No SEP	—	No SEP	—	No SEP	—
2014-06-17 08:29	1198	360	—	S13W123	No SEP	—	No SEP	—	No SEP	—
2014-07-01 23:12	969	84	—	S21E112	No SEP	—	No SEP	—	No SEP	—
2014-07-10 06:56	928	275	C1.9	S14W92	No SEP	—	No data	—	No SEP	—
2014-07-28 13:41	1110	127	C2.4	S08E51	No SEP	—	No SEP	—	No SEP[b]	—
2014-08-08 16:13	1137	360	—	S10W160	No SEP	—	No SEP[b]	—	No SEP	—
2014-09-01 10:48	1901	360	—	N14E127	Good	3.5	No data	—	Good	2777.8
2014-09-01 21:58	1404	360	—	S13E113	HiB_0.3	—	No data	—	HiB_3000	—
2014-09-02 02:10	1141	226	—	S15E114	HiB_0.3	—	No data	—	HiB_3000	—
2014-09-08 23:45	920	360	M4.5	N12E029	HiB_4	—	No data	—	HiB_1	—
2014-09-10 17:00	1071	134	—	N11W169	Multiple	—	No data	—	Multiple	—
2014-09-10 17:27	1267	360	X1.6	N14E002	Contaminated	28.7	No data	—	Good	2.3
2014-09-24 20:50	1350	360	—	N13E179	No SEP	—	No data	—	Contaminated	40.5
2014-09-26 04:15	1469	360	—	S13E111	No SEP	—	No data	—	HiB_200	—
2014-11-01 04:54	1628	159	C2.7	S26E052	Good	4.9	No data	—	No Data	—
2014-12-10 17:56	1086	228	C5.9	S21W104	No SEP	—	No data	—	No Data	—

Table 1 *(continued)*

CME parameters					GOES		STEREO-A		STEREO-B	
launch	speed	width	Flare Class	Flare site	quality	Ip	quality	Ip	quality	Ip
date,time	(km/s)	(deg)				(pfu)		(pfu)		(pfu)
2014-12-12 04:02	1133	127	C1.2	N16W05	No data	—	No data	—	No Data	—
2014-12-13 14:02	2222	360	—	S20W143	No data	—	No data	—	No Data	—
2014-12-18 22:02	1195	360	M6.9	S11E015	No SEP	—	No data	—	No Data	—
2014-12-26 05:10	1097	156	—	S15W110	No SEP	—	No SEP	—	No Data	—
2014-12-30 20:14	902	126	—	S14W147	No SEP	—	No data	—	No Data	—
2015-01-12 15:11	1078	210	C3.7	S12E041	No SEP	—	No data	—	No Data	—
2015-02-09 23:14	1106	360	M2.4	N12E061	No SEP	—	No data	—	No Data	—
2015-02-21 09:18	1120	360	—	S16W164	Good	1.3	No data	—	No Data	—
2015-03-07 21:58	1261	360	M9.2	S19E074	No SEP	—	No data	—	No Data	—
2015-03-09 23:25	995	360	M5.8	S18E045	No SEP	—	No data	—	No Data	—
2015-03-10 03:01	1040	360	M5.1	S15E040	No SEP	—	No data	—	No Data	—
2015-04-21 12:53	1079	83	—	N21E088	No SEP[b]	—	No Data	—	No Data	—
2015-06-09 19:48	1036	262	C2.8	S03E025	No SEP	—	No Data	—	No Data	—
2015-06-14 04:11	1228	195	C5.9	S12W34	No SEP	—	No Data	—	No Data	—
2015-06-18 00:55	1714	195	M1.2	S16W81	Good	16.8	No Data	—	No Data	—
2015-06-18 16:55	1305	360	M3.0	N15E050	HiB_10	—	No Data	—	No Data	—
2015-06-21 02:15	1366	360	M2.6	N12E016	Contaminated	114.0	No Data	—	No Data	—
2015-06-22 17:58	1209	360	M6.5	N12W08	HiB_300	—	No Data	—	No Data	—
2015-06-25 08:17	1627	360	M7.9	N09W42	Good	16.3	No Data	—	No Data	—
2015-09-20 18:00	1239	360	M2.1	S20W24	Good	3.2	No data	—	No Data	—
2015-10-07 07:29	900	145	—	S25W69	No SEP	—	No data	—	No Data	—
2015-11-09 13:06	1041	273	M3.9	S11E041	Good	3.7	No data	—	No Data	—
2015-12-28 11:56	1212	360	M1.8	S23W11	Good	3.7	No SEP	—	No Data	—
2016-01-01 23:15	1730	360	M2.3	S25W82	Good	21.5	No SEP	—	No Data	—
2016-01-06 13:51	969	360	—	S20W133	No SEP	—	No SEP	—	No Data	—
2016-01-29 20:57	901	118	C2.0	S24W66	No SEP	—	No SEP	—	No Data	—
2016-04-18 00:14	1084	162	M6.7	N12W62	No SEP[b]	—	No SEP	—	No Data	—
2016-05-15 15:20	1118	176	C3.2	N10W62	Good	2.2	No SEP	—	No Data	—
2017-04-18 19:27	926	360	C5.5	N14E77	No SEP	—	Good	10.8	No Data	—
2017-07-14 01:12	1200	360	M2.4	S06W29	Good	13.6	No SEP	—	No Data	—
2017-07-23 04:33	1848	360	—	S09W151	No SEP	—	Good	1523.2	No Data	—
2017-09-04 20:21	1418	360	M5.5	S10W12	Good	106.0	No SEP	—	No Data	—
2017-09-06 12:01	1571	360	X9.3	S08W33	HiB_20	[352.0][a]	No SEP	—	No Data	—
2017-09-09 22:33	1019	138	M1.1	S09W89	HiB_1	—	No SEP	—	No Data	—
2017-09-10 15:50	3163	360	X8.2	S09W90	Good	1040.0	Contaminated	6.9	No Data	—
2017-09-17 11:37	1385	360	—	S08E170	No SEP	—	HiB_7	—	No Data	—
2017-10-18 05:24	1576	360	—	S12E122	No SEP	—	Good	5.2	No Data	—

NOTE—

[a] We found a SEP event around the peak even though we missed the onset.

[b] The proton flux increased, but did not reach 1 pfu.

[c] The peak proton flux may be underestimated due to an energetic storm particle (ESP).

Table 2. Timescales of SEP Events

CME parameters						Timescales				
launch	speed	width	Flare site	instrument	quality	Ip	TO	TR	TD	Tm
date,time	(km/s)	(deg)				(pfu)	(min)	(min)	(min)	(min)
2006-12-13 02:25	1774	360	S06W23	GOES	Good	698.0	30.0	180.0	605	420.0
2006-12-14 22:00	1042	360	S06W46	GOES	Good	215.0	65.0	45.0	75	135.0
2010-08-14 09:49	1205	360	N17W52	GOES	Good	14.2	76.0	50.0	280	176.0
2010-08-18 05:29	1471	184	N17W101	GOES	Good	3.7	171.0	70.0	630	321.0
2011-03-07 19:51	2125	360	N30W48	GOES	Good	47.7	114.0	240.0	1415	539.0
2011-03-21 02:13	1341	360	N16W129	GOES	Good	8.0	122.0	180.0	1785	522.0
2011-06-04 21:47	2425	360	N16W153	GOES	Contaminated	4.9	658.0	870.0	—	1818.0
2011-06-07 06:15	1255	360	S21W54	GOES	Good	52.7	65.0	125.0	1115	245.0
2011-08-04 03:39	1315	360	N19W36	GOES	Contaminated	80.1	56.0	150.0	—	411.0
2011-08-08 17:53	1343	237	N16W61	GOES	Good	4.0	57.0	45.0	115	127.0
2011-08-09 07:52	1610	360	N17W69	GOES	Good	26.9	28.0	30.0	465	258.0
2011-09-22 10:33	1905	360	N09E89	GOES	Contaminated	6.8	342.0	785.0	—	1347.0
2011-10-22 10:18	1005	360	N25W77	GOES	Good	4.0	172.0	380.0	3005	767.0
2011-11-03 21:42	991	360	N09E154	GOES	Good	3.7	188.0	405.0	1460	683.0
2011-11-26 06:52	933	360	N17W49	GOES	Good	80.3	88.0	480.0	1330	1113.0
2012-01-19 14:41	1120	360	N32E22	GOES	Good	3.5	1074.0	545.0	570	1749.0
2012-01-23 03:45	2175	360	N28W21	GOES	Contaminated	2820.0	60.0	305.0	—	705.0
2012-01-27 18:18	2508	360	N27W78	GOES	Good	796.0	37.0	230.0	1250	467.0
2012-03-04 10:40	1306	360	N19E61	GOES	Contaminated	3.9	670.0	645.0	—	1790.0
2012-03-07 00:16	2684	360	N17E27	GOES	Contaminated	1630.0	154.0	660.0	—	919.0
2012-03-13 17:20	1884	360	N17W66	GOES	Good	469.0	45.0	65.0	355	205.0
2012-05-17 01:25	1582	360	N11W76	GOES	Good	255.0	30.0	100.0	305	185.0
2012-05-26 20:29	1966	360	N15W121	GOES	Good	14.5	156.0	345.0	495	586.0
2012-07-06 22:54	1828	360	S13W59	GOES	Good	25.2	81.0	230.0	695	531.0
2012-07-17 14:03	958	176	S15W65	GOES	Good	110.0	107.0	240.0	705	547.0
2012-07-23 02:15	2003	360	S17W132	GOES	Good	12.8	320.0	275.0	3790	1170.0
2012-08-31 19:44	1442	360	S19E42	GOES	Good	44.3	341.0	790.0	2015	1586.0
2012-09-27 23:31	947	360	N09W31	GOES	Good	28.4	109.0	140.0	175	314.0
2012-11-08 10:38	972	360	S14W160	GOES	Good	2.4	232.0	765.0	1800	1062.0
2013-03-15 06:42	1063	360	N11E012	GOES	Good	14.7	763.0	900.0	1435	2348.0
2013-04-21 07:10	919	360	N10W119	GOES	Good	3.3	165.0	70.0	1440	570.0
2013-05-13 15:47	1850	360	N11E85	GOES	Contaminated	1.3	323.0	205.0	—	1018.0
2013-05-15 01:27	1366	360	N12E64	GOES	Good	22.0	288.0	435.0	2450	1048.0
2013-05-22 12:55	1466	360	N15W70	GOES	Good	1650.0	65.0	660.0	670	1010.0
2013-06-21 02:53	1900	207	S16E73	GOES	Good	6.7	707.0	475.0	1570	1797.0
2013-09-29 21:52	1179	360	N17W29	GOES	Good	182.0	138.0	775.0	1825	1333.0
2013-10-28 04:16	1201	156	N08W71	GOES	Contaminated	4.0	139.0	225.0	—	1014.0
2013-11-06 23:25	1033	360	S11W97	GOES	Good	6.7	155.0	55.0	455	310.0
2013-12-26 03:02	1336	360	S09E166	GOES	Good	2.7	358.0	495.0	1630	1428.0
2013-12-28 17:09	1118	360	S15W125	GOES	Good	29.3	121.0	180.0	370	366.0
2014-01-06 07:33	1402	360	S15W112	GOES	Good	40.1	42.0	100.0	1380	282.0
2014-02-20 07:28	948	360	S15W73	GOES	Good	22.3	52.0	35.0	150	117.0
2014-02-25 00:32	2147	360	S12E82	GOES	Contaminated	23.9	183.0	685.0	—	1418.0
2014-04-18 12:43	1203	360	S20W34	GOES	Contaminated	58.5	62.0	330.0	—	742.0
2014-09-01 10:48	1901	360	N14E127	GOES	Good	3.5	677.0	1175.0	10495	3402.0
2014-09-10 17:27	1267	360	N14E002	GOES	Contaminated	28.7	248.0	345.0	—	708.0
2014-11-01 04:54	1628	159	S26E052	GOES	Good	4.9	541.0	270.0	2600	921.0
2015-02-21 09:18	1120	360	S16W164	GOES	Good	1.3	312.0	85.0	2240	607.0
2015-06-18 00:55	1714	195	S16W81	GOES	Good	16.8	200.0	285.0	1365	830.0

Table 2 *continued on next page*

Table 2 *(continued)*

CME parameters						Timescales				
launch	speed	width	Flare site	instrument	quality	Ip	TO	TR	TD	Tm
date,time	(km/s)	(deg)				(pfu)	(min)	(min)	(min)	(min)
2015-06-21 02:15	1366	360	N12E016	GOES	Contaminated	114.0	70.0	1290.0	—	1540.0
2015-06-25 08:17	1627	360	N09W42	GOES	Good	16.3	103.0	885.0	2160	1563.0
2015-09-20 18:00	1239	360	S20W24	GOES	Good	3.2	75.0	75.0	185	165.0
2015-11-09 13:06	1041	273	S11E041	GOES	Good	3.7	404.0	215.0	385	674.0
2015-12-28 11:56	1212	360	S23W11	GOES	Good	3.7	144.0	570.0	395	834.0
2016-01-01 23:15	1730	360	S25W82	GOES	Good	21.5	60.0	255.0	200	335.0
2016-05-15 15:20	1118	176	N10W62	GOES	Good	2.2	195.0	145.0	245	360.0
2017-07-14 01:12	1200	360	S06W29	GOES	Good	13.6	158.0	140.0	1860	583.0
2017-09-04 20:21	1418	360	S10W12	GOES	Good	106.0	129.0	280.0	1415	659.0
2017-09-10 15:50	3163	360	S09W90	GOES	Good	1040.0	35.0	85.0	2075	175.0
2006-12-13 02:25	1774	360	S06W23	STEREO-A	Good	592.1	42.5	155.0	705	372.5
2010-08-18 05:29	1471	184	N17W101	STEREO-A	Good	3.7	78.5	145.0	190	228.5
2010-08-31 20:40	1304	360	S22W146	STEREO-A	Good	1.2	132.5	140.0	530	377.5
2011-03-07 19:51	2125	360	N30W48	STEREO-A	Contaminated	62.4	361.5	1845.0	—	2266.5
2011-03-21 02:13	1341	360	N16W129	STEREO-A	Good	1102.9	39.5	80.0	320	159.5
2011-03-29 20:14	1264	195	N20E117	STEREO-A	Good	1.2	518.5	470.0	550	1168.5
2011-06-04 06:26	1407	360	N16W144	STEREO-A	Contaminated	159.2	136.5	475.0	—	646.5
2011-09-22 10:33	1905	360	N09E89	STEREO-A	Good	11.0	304.5	610.0	1865	984.5
2011-10-04 12:32	1101	360	N26E153	STEREO-A	Good	4.8	210.5	405.0	1570	880.5
2011-11-03 21:42	991	360	N09E154	STEREO-A	Good	210.5	80.5	125.0	320	315.5
2011-11-26 06:52	933	360	N17W49	STEREO-A	Good	17.4	510.5	1015.0	1005	2295.5
2012-01-23 03:45	2175	360	N28W21	STEREO-A	Good	48.4	357.5	1585.0	3350	2297.5
2012-03-07 00:16	2684	360	N17E27	STEREO-A	Contaminated	5.8	196.5	500.0	—	1686.5
2012-03-18 00:04	1210	360	N18W116	STEREO-A	Contaminated	3.0	178.5	55.0	—	318.5
2012-03-21 07:12	1178	360	N18W160	STEREO-A	Good	58.1	75.5	85.0	515	315.5
2012-03-23 23:58	1152	360	N18E164	STEREO-A	Good	138.3	54.5	75.0	165	179.5
2012-05-17 01:25[a]	1582	360	N11W76	STEREO-A	Contaminated	2.7	647.5	1015.0	—	2107.5
2012-05-26 20:29	1966	360	N15W121	STEREO-A	Contaminated	13.5	58.5	45.0	—	113.5
2012-07-23 02:15	2003	360	S17W132	STEREO-A	Good	49778.4	62.5	995.0	160	1117.5
2012-09-27 09:57	1319	360	S25W151	STEREO-A	Contaminated	95.4	85.5	130.0	—	220.5
2012-10-14 00:14	987	360	N13E137	STEREO-A	Good	3.2	83.5	65.0	1040	323.5
2012-11-08 10:38	972	360	S14W160	STEREO-A	Good	37.3	39.5	80.0	2560	269.5
2012-11-23 23:00	1186	360	N14W130	STEREO-A	Good	5.1	117.5	575.0	655	927.5
2013-03-05 03:23	1316	360	N10E144	STEREO-A	Good	1849.9	29.5	120.0	790	354.5
2013-05-22 12:55	1466	360	N15W70	STEREO-A	Contaminated	4.2	517.5	315.0	—	977.5
2013-07-22 05:57	1004	360	N16W155	STEREO-A	Good	5.3	95.5	125.0	235	260.5
2013-10-05 06:41	964	360	S22E118	STEREO-A	Good	42.9	86.5	380.0	715	756.5
2013-10-11 07:05	1200	360	N21E103	STEREO-A	Good	218.5	42.5	80.0	385	237.5
2013-11-07 10:03	1405	360	N02E151	STEREO-A	Good	73.9	54.5	50.0	725	249.5
2013-12-26 03:02	1336	360	S09E166	STEREO-A	Good	54.6	115.5	390.0	1375	660.5
2014-01-21 20:41	1065	221	S13E162	STEREO-A	Good	3.7	166.5	325.0	695	521.5
2014-02-09 15:38	908	360	S15E103	STEREO-A	Good	2.0	124.5	40.0	435	244.5
2014-02-25 00:32	2147	360	S12E82	STEREO-A	Good	205.2	60.5	115.0	825	325.5
2014-03-12 14:08	972	360	N18E158	STEREO-A	Good	46.1	69.5	70.0	110	164.5
2017-04-18 19:27	926	360	N14E77	STEREO-A	Good	10.8	110.5	115.0	635	310.5
2017-07-23 04:33	1848	360	S09W151	STEREO-A	Good	1523.2	149.5	925.0	1390	1519.5
2017-09-10 15:50	3163	360	S09W90	STEREO-A	Contaminated	6.9	907.5	1630.0	—	2702.5
2017-10-18 05:24	1576	360	S12E122	STEREO-A	Good	5.2	93.5	690.0	1100	973.5
2006-12-13 02:25	1774	360	S06W23	STEREO-B	Good	567.4	37.5	165.0	705	342.5
2011-03-29 20:14	1264	195	N20E117	STEREO-B	Good	4.1	703.5	770.0	1595	1578.5
2011-05-09 20:39	1318	292	N18E93	STEREO-B	Good	1.3	213.5	265.0	725	598.5

Table 2 *(continued)*

CME parameters							Timescales				
launch	speed	width	Flare site	instrument	quality	Ip	TO	TR	TD	Tm	
date,time	(km/s)	(deg)				(pfu)	(min)	(min)	(min)	(min)	
2011-06-04 21:47	2425	360	N16W153	STEREO-B	Good	20.7	755.5	3115.0	5350	5285.5	
2011-09-22 10:33	1905	360	N09E89	STEREO-B	Good	2095.7	44.5	520.0	1875	989.5	
2011-10-04 12:32	1101	360	N26E153	STEREO-B	Good	20.7	160.5	170.0	675	530.5	
2011-11-03 21:42	991	360	N09E154	STEREO-B	Good	4.1	110.5	85.0	1730	250.5	
2011-11-17 20:15	1041	360	N18E120	STEREO-B	Good	3.1	262.5	370.0	655	827.5	
2012-01-16 02:54	1060	360	N34E86	STEREO-B	Good	1.6	358.5	1295.0	1885	1803.5	
2012-01-19 14:41	1120	360	N32E22	STEREO-B	Good	17.0	186.5	365.0	1595	776.5	
2012-01-23 03:45	2175	360	N28W21	STEREO-B	Good	55.1	137.5	190.0	2610	377.5	
2012-03-04 10:40	1306	360	N19E61	STEREO-B	Good	209.6	262.5	500.0	355	927.5	
2012-03-07 00:16	2684	360	N17E27	STEREO-B	Contaminated	233.7	71.5	85.0	—	221.5	
2012-03-23 23:58	1152	360	N18E164	STEREO-B	Contaminated	2.6	384.5	355.0	—	854.5	
2012-07-02 08:03	1074	360	S16E134	STEREO-B	Good	7.0	834.5	1610.0	335	2574.5	
2012-07-23 02:15	2003	360	S17W132	STEREO-B	Good	31.0	957.5	1460.0	5335	2942.5	
2012-08-31 19:44	1442	360	S19E42	STEREO-B	Good	999.9	53.5	495.0	1430	1053.5	
2012-09-20 14:31	1202	360	S15E155	STEREO-B	Contaminated	12.3	46.5	830.0	—	1171.5	
2012-09-27 23:31	947	360	N09W31	STEREO-B	Good	22.3	191.5	160.0	160	386.5	
2013-03-05 03:23	1316	360	N10E144	STEREO-B	Good	140.8	134.5	2475.0	895	3409.5	
2013-05-13 02:00	1270	360	N11E90	STEREO-B	Good	17.8	72.5	65.0	255	217.5	
2013-05-13 15:47	1850	360	N11E85	STEREO-B	Contaminated	108.3	95.5	110.0	—	300.5	
2013-06-21 02:53	1900	207	S16E73	STEREO-B	Good	51.4	94.5	155.0	1115	469.5	
2013-08-30 02:04	949	360	N15E46	STEREO-B	Good	4.1	103.5	95.0	350	293.5	
2013-09-29 21:52	1179	360	N17W29	STEREO-B	Good	1.0	640.5	505.0	1510	1475.5	
2013-10-05 06:41	964	360	S22E118	STEREO-B	Good	2.3	596.5	840.0	1740	1996.5	
2013-10-11 07:05	1200	360	N21E103	STEREO-B	Good	21.8	72.5	215.0	2005	682.5	
2013-10-28 13:44	1073	93	N06W75	STEREO-B	Good	7.8	183.5	245.0	930	1138.5	
2013-11-07 10:03	1405	360	N02E151	STEREO-B	Good	997.5	79.5	345.0	1360	704.5	
2013-12-26 03:02	1336	360	S09E166	STEREO-B	Good	59.4	100.5	355.0	2300	750.5	
2014-01-07 18:04	1830	360	S15W11	STEREO-B	Good	6.7	253.5	1395.0	1390	2023.5	
2014-02-21 15:28	1252	360	S15E121	STEREO-B	Good	16.1	74.5	170.0	1115	539.5	
2014-02-25 00:32	2147	360	S12E82	STEREO-B	Good	316.7	65.5	185.0	2445	610.5	
2014-03-12 14:08	972	360	N18E158	STEREO-B	Good	4.7	129.5	290.0	800	719.5	
2014-04-02 13:22	1471	360	N11E53	STEREO-B	Good	184.4	120.5	55.0	315	220.5	
2014-06-10 12:44	1469	360	S17E82	STEREO-B	Good	12.3	128.5	140.0	445	388.5	
2014-09-01 10:48	1901	360	N14E127	STEREO-B	Good	2777.8	49.5	140.0	1925	489.5	
2014-09-10 17:27	1267	360	N14E002	STEREO-B	Good	2.3	220.5	205.0	1815	955.5	
2014-09-24 20:50	1350	360	N13E179	STEREO-B	Contaminated	40.5	92.5	385.0	—	677.5	

NOTE—

[a] Peak proton flux and timescales may be underestimated due to an energetic storm particle (ESP).

REFERENCES

Anastasiadis, A., Papaioannou, A., Sandberg, I., et al. 2017, SoPh, 292, 134, doi: 10.1007/s11207-017-1163-7

Brueckner, G. E., Howard, R. A., Koomen, M. J., et al. 1995, SoPh, 162, 357, doi: 10.1007/BF00733434

Burkepile, J. T., Hundhausen, A. J., Stanger, A. L., St. Cyr, O. C., & Seiden, J. A. 2004, Journal of Geophysical Research (Space Physics), 109, A03103, doi: 10.1029/2003JA010149

Cane, H. V., Erickson, W. C., & Prestage, N. P. 2002, Journal of Geophysical Research (Space Physics), 107, 1315, doi: 10.1029/2001JA000320

Cane, H. V., Reames, D. V., & von Rosenvinge, T. T. 1988, J. Geophys. Res., 93, 9555, doi: 10.1029/JA093iA09p09555

Cliver, E. W. 1982, SoPh, 75, 341, doi: 10.1007/BF00153481

—. 2016, ApJ, 832, 128, doi: 10.3847/0004-637X/832/2/128

22

Desai, M., & Giacalone, J. 2016, Living Reviews in Solar Physics, 13, 3, doi: 10.1007/s41116-016-0002-5

Dierckxsens, M., Tziotziou, K., Dalla, S., et al. 2015, SoPh, 290, 841, doi: 10.1007/s11207-014-0641-4

Gómez-Herrero, R., Dresing, N., Klassen, A., et al. 2015, ApJ, 799, 55, doi: 10.1088/0004-637X/799/1/55

Gopalswamy, N., Xie, H., Akiyama, S., et al. 2013, ApJL, 765, L30, doi: 10.1088/2041-8205/765/2/L30

Gopalswamy, N., Yashiro, S., Krucker, S., Stenborg, G., & Howard, R. A. 2004, Journal of Geophysical Research (Space Physics), 109, A12105, doi: 10.1029/2004JA010602

Gopalswamy, N., Yashiro, S., Thakur, N., et al. 2016, ApJ, 833, 216, doi: 10.3847/1538-4357/833/2/216

Gosling, J. T. 1993, J. Geophys. Res., 98, 18937, doi: 10.1029/93JA01896

Grechnev, V. V., Kiselev, V. I., Meshalkina, N. S., & Chertok, I. M. 2015, SoPh, 290, 2827, doi: 10.1007/s11207-015-0797-6

Guo, J., Dumbović, M., Wimmer-Schweingruber, R. F., et al. 2018, Space Weather, 16, 1156, doi: 10.1029/2018SW001973

Hudson, H. S., & Cliver, E. W. 2001, J. Geophys. Res., 106, 25199, doi: 10.1029/2000JA904026

Iwai, K., Yashiro, S., Nitta, N. V., & Kubo, Y. 2020, ApJ, 888, 50, doi: 10.3847/1538-4357/ab57ff

Kahler, S. W. 1982, J. Geophys. Res., 87, 3439, doi: 10.1029/JA087iA05p03439

—. 2001, J. Geophys. Res., 106, 20947, doi: 10.1029/2000JA002231

—. 2005, ApJ, 628, 1014, doi: 10.1086/431194

—. 2013, ApJ, 769, 110, doi: 10.1088/0004-637X/769/2/110

Kahler, S. W., Hildner, E., & Van Hollebeke, M. A. I. 1978, SoPh, 57, 429, doi: 10.1007/BF00160116

Kahler, S. W., Reames, D. V., & Sheeley, N. R., J. 2001, ApJ, 562, 558, doi: 10.1086/323847

Kahler, S. W., Sheeley, N. R., J., Howard, R. A., et al. 1984, J. Geophys. Res., 89, 9683, doi: 10.1029/JA089iA11p09683

Kahler, S. W., & Vourlidas, A. 2005, Journal of Geophysical Research (Space Physics), 110, A12S01, doi: 10.1029/2005JA011073

Kouloumvakos, A., Rouillard, A. P., Wu, Y., et al. 2019, ApJ, 876, 80, doi: 10.3847/1538-4357/ab15d7

Lario, D., Kwon, R. Y., Balmaceda, L., et al. 2020, ApJ, 889, 92, doi: 10.3847/1538-4357/ab64e1

Laurenza, M., Cliver, E. W., Hewitt, J., et al. 2009, Space Weather, 7, S04008, doi: 10.1029/2007SW000379

Lee, M. A., Mewaldt, R. A., & Giacalone, J. 2012, SSRv, 173, 247, doi: 10.1007/s11214-012-9932-y

Li, G., & Zank, G. P. 2005, in International Cosmic Ray Conference, Vol. 1, 29th International Cosmic Ray Conference (ICRC29), Volume 1, 173

Lin, R. P., & Hudson, H. S. 1976, SoPh, 50, 153, doi: 10.1007/BF00206199

Luhmann, J. G., Curtis, D. W., Schroeder, P., et al. 2008, SSRv, 136, 117, doi: 10.1007/s11214-007-9170-x

Mewaldt, R. A., Cohen, C. M. S., Cook, W. R., et al. 2008, SSRv, 136, 285, doi: 10.1007/s11214-007-9288-x

Miller, J. A., Cargill, P. J., Emslie, A. G., et al. 1997, J. Geophys. Res., 102, 14631, doi: 10.1029/97JA00976

Nitta, N. V., Aschwanden, M. J., Freeland, S. L., et al. 2014, SoPh, 289, 1257, doi: 10.1007/s11207-013-0388-3

Onsager, T., Grubb, R., Kunches, J., et al. 1996, Society of Photo-Optical Instrumentation Engineers (SPIE) Conference Series, Vol. 2812, Operational uses of the GOES energetic particle detectors, ed. E. R. Washwell, 281–290, doi: 10.1117/12.254075

Pan, Z. H., Wang, C. B., Wang, Y., & Xue, X. H. 2011, SoPh, 270, 593, doi: 10.1007/s11207-011-9763-0

Papaioannou, A., Sandberg, I., Anastasiadis, A., et al. 2016, Journal of Space Weather and Space Climate, 6, A42, doi: 10.1051/swsc/2016035

Pesnell, W. D., Thompson, B. J., & Chamberlin, P. C. 2012, SoPh, 275, 3, doi: 10.1007/s11207-011-9841-3

Reames, D. V. 1999, SSRv, 90, 413, doi: 10.1023/A:1005105831781

—. 2013, SSRv, 175, 53, doi: 10.1007/s11214-013-9958-9

Richardson, I. G., von Rosenvinge, T. T., Cane, H. V., et al. 2014, SoPh, 289, 3059, doi: 10.1007/s11207-014-0524-8

Rodriguez, J. V., Sandberg, I., Mewaldt, R. A., Daglis, I. A., & Jiggens, P. 2017, Space Weather, 15, 290, doi: 10.1002/2016SW001533

Smart, D. F., & Shea, M. A. 1996, Advances in Space Research, 17, 113, doi: 10.1016/0273-1177(95)00520-O

Sun, X., Bobra, M. G., Hoeksema, J. T., et al. 2015, ApJL, 804, L28, doi: 10.1088/2041-8205/804/2/L28

Thernisien, A. F. R., Howard, R. A., & Vourlidas, A. 2006, ApJ, 652, 763, doi: 10.1086/508254

Trottet, G., Samwel, S., Klein, K. L., Dudok de Wit, T., & Miteva, R. 2015, SoPh, 290, 819, doi: 10.1007/s11207-014-0628-1

Van Hollebeke, M. A. I., Ma Sung, L. S., & McDonald, F. B. 1975, SoPh, 41, 189, doi: 10.1007/BF00152967

von Rosenvinge, T. T., Reames, D. V., Baker, R., et al. 2008, SSRv, 136, 391, doi: 10.1007/s11214-007-9300-5

Xie, H., Ofman, L., & Lawrence, G. 2004, Journal of Geophysical Research (Space Physics), 109, A03109, doi: 10.1029/2003JA010226

Yashiro, S., Gopalswamy, N., Michalek, G., et al. 2004, Journal of Geophysical Research (Space Physics), 109, A07105, doi: 10.1029/2003JA010282

Zhang, J., Richardson, I. G., Webb, D. F., et al. 2007, Journal of Geophysical Research (Space Physics), 112, A10102, doi: 10.1029/2007JA012321

Zhang, M., Qin, G., & Rassoul, H. 2009, ApJ, 692, 109, doi: 10.1088/0004-637X/692/1/109